VITRIMER-BASED ADHESIVES FOR FULLY REVERSIBLE JOINTS

by

MORGAN ANN DECROIX

A thesis submitted in partial fulfillment of the
requirements for the degree of

MASTER OF SCIENCE IN MECHANICAL ENGINEERING

2026

Oakland University
Rochester, Michigan

Thesis Advisory Committee:

Marco Gerini-Romagnoli, Ph.D., Chair
Zhijun Wu, Ph.D.
Aaqib Ali, Ph.D.
Wenbo Wang, Ph.D.
Tequila Harris, Ph.D.

To my adviser, family, and Alexandru.

ACKNOWLEDGMENTS

First, I would like express my sincere thanks to my adviser, Dr. Marco Gerini-Romagnoli, for his support during this process, and for helping me to become a more capable and confident student. The environment created by Dr. G. has pushed me out of my comfort zone, providing opportunities for academic and professional development. I am deeply grateful for the knowledge and experience that I gained under his guidance.

I also want to express my sincere gratitude to my committee members: Drs. Aaqib Ali, Tequila Harris, Wenbo Wang, and Zhijun Wu, for their guidance and support. Their constructive feedback has helped improve the quality of this research work.

Thank you also to the faculty and collaborators from the center for Composite and Hybrid Material Interfacing (CHMI): Dr. Sayed Nassar (OU Site PI of CHMI), Dr. Donggang Yao, the graduate students at Georgia Tech, and to the Industry Advisory Board (IAB) members who have helped shape this work.

A special thank you goes to Dr. Xia Wang, who has supported my academic development throughout my undergraduate and graduate programs. Without her advocating for me, I would not have had any of the opportunities that have shaped my academic past, present, and future.

Lastly, I want to thank my friends and family – mom, dad, siblings, and my niece, Beverly – for their inspiration and continued support. Most of all, thank you to my fiancé , Alex, for all that you have done to make this possible and for motivating me to be a better version of myself.

MORGAN ANN DECROIX

ABSTRACT

VITRIMER-BASED ADHESIVES FOR FULLY REVERSIBLE JOINTS

by

MORGAN ANN DECROIX

Adviser: Marco Gerini-Romagnoli, Ph.D.

The permanent nature of structural adhesive joints impairs repair, reuse, and recycling of bonded components and structures. In recent years the development of alternative, controlled de-bonding methods that aim to facilitate part disassembly and recovery has accelerated. The properties of vitrimer-based polymers can be harnessed to improve the sustainability of adhesive bonding by enabling full reversibility of structural bonded joints.

In this study, the properties of two vitrimer formulations – abbreviated as VA.1 and VA.2, respectively – are studied for their application as structural adhesives. The first vitrimer is synthesized from diglycidyl 1,2-cyclohexanedicarboxylate (DCN) and internally catalyzed by the curing agent polyethylenimine (PEI), while the second formulation is commercially available, and is purchased directly from the manufacturer. Mechanical, environmental aging/durability, and reversibility tests are performed. The viscoelastic properties of the vitrimers are measured with Dynamic Mechanical Analysis (DMA) and are used to determine the glass transition temperature (T_g), which gives the adhesive's operational temperature ceiling.

Both formulations exhibit reasonable thermomechanical stability, yielding viscoelastic properties dependent on (i) constituent mix ratio, (ii) curing schedule, and (iii) environmental loading history. Bulk material specimens and aluminum alloy and

multi-material (aluminum alloy + carbon fiber composite) single lap joints (SLJs) are fabricated to investigate strength and durability through lap shear testing, creep, relaxation, and hot-wet/submersion tests. Furthermore, SLJs undergo reversibility testing by means of electromagnetic excitation of the substrates for de-bonding under constant 100 N load and welding/re-bonding. Experimental results on the viability of vitrimer-based adhesives for fully reversible structural joints are presented and discussed.

In *Chapter 1*, a broad introduction and review of the literature is included. The following areas are surveyed: the current state-of-the-art for joint de-bonding, advances in the research on covalent adaptable network (vitrimer) materials, and the use of vitrimers as de-bondable adhesives. Several research gaps are identified: as of the time of writing this thesis, vitrimer research is less than 2 decades old. At the end of the chapter, the thesis objectives are outlined.

In *Chapter 2*, the 2 vitrimer formulations used in this thesis are described with the relevant literature studies. Joint substrate materials and test specimens geometry are defined.

In *Chapter 3*, the experimental setup and methodology are discussed. The synthesis steps for both vitrimer formulations are outlined. The joint fabrication process and the methodology for (i) lap shear, (ii) creep, and (iii) fracture toughness testing are described. Dynamic Mechanical Analysis and environmental aging parameters for bulk material characterization are reported for the tested vitrimer configurations. Finally, the procedure for de-bonding and welding/re-bonding tests is outlined.

In *Chapter 4*, results are presented and discussed. The lap shear strength and glass transition temperature of both formulations are comparable to commercial structural adhesives: up to 16.5 MPa and 53 °C for VA.1, and 18.0 MPa and 101 °C for VA.2. The DCN-PEI (VA.1) vitrimer is very hygroscopic, reaching 49% moisture uptake upon submersion in de-ionized water. VA.1 viscoelastic moduli drop by 1 order of magnitude

after hot/wet storage + drying, but fully recover upon healing at high temperature. The fracture toughness of VA.1 (1.8 kJ/m^2) is measured using tapered double cantilever beam specimens, and is comparable to typical toughened epoxies. De-bonding is highly repeatable for all tested variations: all joints de-bond in less than 5 min. Re-bonding and/or welding is more effective for VA.2 joints, which reach as high as 53% healing efficiency, while self-welding of VA.1 joints only yields a strength equal to 20% of the baseline lap shear strength.

In *Chapter 5*, conclusions are discussed. Additionally, the novel findings are summarized, as well as detailed recommendations for future work.

This thesis is made possible by the generous support of the National Science Foundation under Grant No. 2052658.

TABLE OF CONTENTS

TABLE OF CONTENTS—Continued

TABLE OF CONTENTS—Continued

LIST OF TABLES

LIST OF FIGURES

LIST OF ABBREVIATIONS

D	diffusivity
E”	Loss Modulus
E	Modulus of Elasticity
E'	Storage Modulus
E'_r	Rubbery Modulus
G_{1a}	opening mode crack arrest toughness (energy release rate)
G_{1c}	opening mode fracture toughness (energy release rate)
I	Current
M_∞	peak saturation
S_{ut}	tensile strength
T_g	glass transition temperature
T_v	network topology freezing temperature
V	Voltage
ρ_v	crosslink density
τ	relaxation time
f	frequency
$T_{de\text{-}bond}$	de-bonding temperature
$t_{de\text{-}bond}$	de-bonding time
3Rs	Repair, Recovery, and Recycling
AA	Aluminum Alloy

CAN	Covalent Adaptable Network
CFRP	Carbon Fiber-Reinforced Plastic
DCN	diglycidyl 1,2-cyclohexanedicarboxylate
DGEBA	diglycidyl ether of Bisphenol A
DMA	Dynamic Mechanical Analysis
DSC	Digital Scanning Calorimetry
EoL	End-of-Life
FRP	Fiber-Reinforced Plastic
HMA	Hot-Melt Adhesive
IH	Induction Heating
LSS	Lap Shear Strength
MNP	Magnetically Active Nanoparticle
PEI	polyethylenimine
PTFE	Polytetrafluoroethylene
RB	Re-bonding
RH	Relative Humidity
SFE	Surface Free Energy
SLJ	Single Lap Joint
SW	Self-Welding
TDCB	Tapered Double Cantilever Beam
TEP	Thermally Expandable Particle

CHAPTER ONE

INTRODUCTION AND LITERATURE REVIEW

This chapter contains a high-level overview of adhesives and adhesive bonding research and technology, as well as a summary of socioeconomic and environmental factors promoting the development of easily de-bondable adhesives. Current methods for on-demand de-bonding by particle additives (thermally expandable particles and magnetic nanoparticles) or non-structural hot-melt adhesives and the relevant studies are summarized. The characteristics of vitrimers as a whole, common vitrimer applications and recycling methods, and the current research involving vitrimers as adhesives are summarized. Finally, the thesis objectives and the research gaps that inform this study are introduced.

1.1 Motivation for de-bondable adhesive joints

Environmental damage caused by greenhouse gas emissions and exacerbated by linear economic practices has prompted stricter regulatory policies on the transportation sector, calling for improved recyclability of motor vehicles and fuel efficiency standards [1, 2]. A prime example of waste mitigation efforts is seen in the European Union End-of-Life Vehicle Directive [3], which requires all vehicles manufactured after 2015 be at least 95% recyclable by weight. More broadly, to achieve climate neutrality, a 90% reduction in greenhouse gas emissions is needed by the year 2050 [4]. Vehicle design is being shaped by increasingly aggressive regulations like those imposed in the European Union in the transportation sector [1, 5]. A comprehensive study by Candela et al. [6] shows that vehicle light-weighting is an effective method to reduce energy consumption ($\sim$6% increased fuel efficiency per 10% weight decrease [7]). The current industry shift towards electrification for passenger and commercial vehicles highlights the importance of

light-weighting due to the necessity to offset the weight of batteries to meet weight standards and extend battery life.

To facilitate meeting these standards, adhesive bonding has become commonplace in the automotive and aerospace industries. Adhesives are a primary methods for materials joining alongside welds, rivets, and bolts. As opposed to mechanical fasteners, a few notable benefits of adhesive bonding are [8, 9, 7]:

- High strength-to-weight ratio.
- High stiffness-to-weight ratio.
- Thermal and vibratory insulation.
- Galvanic corrosion prevention via isolation of dissimilar materials (e.g. steel-to-aluminum or aluminum-to-composites).
- More uniform stress distribution.
- Increased design flexibility for effective light-weighting.
- Excellent fatigue strength.

Adhesive bonding allows to isolate dissimilar materials, thereby helping to prevent galvanic corrosion in humid environments [10, 11]. Moreover, adhesives are especially important as they are the preferred joining method for fiber-reinforced composites (FRPs), because they do not necessitate drilling of substrates, which causes fiber discontinuities that increase susceptibility to failure (e.g. failure by delamination) [12].

Despite the many draws towards adhesives, they are not perfectly fit for all applications. Some of the main disadvantages, as compared to welded, bolted, or riveted joints, include:

- Once fully cured, the cross-linked networks are permanent.

- Lower environmental stability (dependent on adhesive chemistry).
- Energy intense surface preparation and cure process.
- Difficult or impossible inspection or repair.

The thermoset-nature of adhesives means that they are inherently non-reprocessable. Therefore, the savings brought by extensive structural adhesive usage in vehicles and lightweight assemblies are at least partially offset by the often difficult and cost-ineffective Repair, Recovery, and Recycling (3Rs) of bonded structures [2]. In particular, End-of-Life (EoL) activities are negatively affected by structural bonding – especially in the case of joints between dissimilar materials. Current industry practices for disassembling bonded structures typically require the mechanical grinding of substrates or extreme loads/heat – both of which inhibit recovery and recyclability [13].

1.2 Adhesion and adhesives background

The precise mechanisms of adhesion are still not fully understood. Established adhesion theories include: the adsorption theory, the mechanical theory (mechanical interlocking), and the electrostatic theory [14]. The common consensus is that adhesion involves some combination of all three theories, which explains why effective bonding relies on the good wetting (coverage) of the substrates, as well as the adhesive's gap filling capabilities. These properties can be optimized by tuning adhesive viscosity (between 10^4 and 10^6 cP) [15]. Adhesion can also be enhanced by increasing Surface Free Energy (SFE) of the substrate with surface preparation techniques like mechanical abrasion, sand-blasting, chemical etching, and degreasing agents [16].

Commercially available structural adhesives – such as those commonly used in automotive, aerospace, and other critical sectors – must meet certain engineering design requirements like strength, toughness, operating temperature, and durability. Joint

strength is typically tested using SLJs; this is because adhesives perform best while loaded predominantly in shear. During lap shear testing, the SLJ is pulled until failure, and the maximum joint load normalized over the bond area is called the Lap Shear Strength (LSS) [17]. In Table 1.1, structural epoxy adhesives currently on the market and their substrates, surface preparation, lap shear strength, and reported glass transition temperature (T_g) are summarized and to give a baseline for typical properties.

Structural adhesives are predominantly thermosetting resins because their cross-linked network lends itself to excellent mechanical properties and thermomechanical stability [18]. Epoxies are the most important type of structural adhesives due their their versatility, high strength, chemical resistance, and thermomechanical stability. Unmodified epoxies are brittle and have low toughness ($\sim$0.1-0.5 kJ/m^2); however, they display excellent thermal resistance (up to 260 °C for short periods) and a typical service temperature between -55-121 °C [19]. The

Table 1.1: Properties of commercially available toughened epoxy adhesives

Adhesive	Substrates	LSS	T_g
3M™ Scotch-Weld™ Toughened Epoxy Adhesive LSB60	Aluminum	25 MPa (3.6 ksi)	53°C (127°F)
Araldite 2011 Structural Adhesive	Aluminum	19 MPa (2.8 ksi)	45°C (113°F)
9201 – Structural Epoxy Adhesive	Aluminum	26 MPa (3.8 ksi)	42°C (107°F)
PERMABOND ET5441	Aluminum	19 MPa (2.8 ksi)	113°C (235°F)
EPIBOND 315 A/B	Aluminum 2024	38 MPa (5.5 ksi)	125°C (260°F)

commercially available toughened epoxies detailed in Table 1.1 demonstrate the high strength (19-25 MPa) and high T_g (with operating temperature being slightly higher). Epoxy adhesives can have LSS as low as 7 MPa (1 ksi) or as high as 50 MPa (7 ksi) depending on the chemistry and substrate material. Other common types of structural adhesives are polyurethanes and acrylics. Both types typically feature lower strength and stability than high-strength epoxies, but have other properties (such as polyurethanes' ductility or acrylics' fast cure) that make them better suited for specific applications [19].

1.3 Current state-of-the art for de-bonding

In response to the previously mentioned regulations and economic drivers, methodologies for on-demand de-bonding have emerged [20]. A few of those methodologies include: employing micro- or nano- particle additives, hot-melt adhesives, and solvent-based adhesive swelling [20, 21]. An ideal method for on-demand de-bonding (to facilitate the 3Rs as discussed in Section 1.1) would aid joint separation without altering the adhesive performance during typical usage conditions, promoting strength loss upon the application of an intentional external stimulus. This ensures that the permanent degradation of material properties of the substrates during 3R activities is avoided.

1.3.1 Thermally expandable (micro)particles for additive-based de-bonding

Thermally Expandable Particles (TEPs) are encapsulated gas microspheres with a copolymer shell, which can be used as adhesive additives to assist fast, heat-driven de-bonding via crack propagation in the adhesive layer. Upon heating, the combined action of the TEPs' shell softening and the gasification of the encapsulated liquid hydrocarbon allow the microparticles to expand anywhere from 50 to 100 times their original volume. The temperature at which expansion starts (T_{start}) and the temperature of maximum volumetric expansion (T_{max}) vary depending on the particle size, type, and

grade. Typical activation and maximum expansion temperatures range from 70 °C to 285 °C [20].

Banea et al. have extensively explored the performance of TEP-modified adhesives in several studies, which include: an initial characterization of strength and thermal properties of tool steel SLJs with a structural polyurethane adhesive to demonstrate proof of concept [22], an investigation of bulk properties of TEP-modified polyurethane and epoxy adhesive systems commonly used in the automotive sector [23], assessment of LSS and de-bonding (performed via heating of the joint via electromagnetic excitation with an induction coil) performance of the two adhesives mentioned in the previous study with steel SLJs and multi-material (Aluminum-CFRP) substrates [24, 25], and an investigation of the impact of water-absorption on mechanical and de-bonding performance [26]. For one of the tested adhesives, optimal joint strength and de-bonding performance was achieved with 15 wt.% TEP loading, which corresponded to a 27% decrease in LSS, to a de-bonding time ($t_{de\text{-}bond}$) of less than 80 s, and a de-bonding temperature ($T_{de\text{-}bond}$) of $\sim$145 °C [24]. A key takeaway from these studies is that the addition of TEPs to commercially available adhesives systems – polyurethane and epoxy – can promote fast on-demand de-bonding at low loads. Furthermore, the addition of TEPs to compatible paste adhesives did not dramatically degrade joint strength and stability, while low-load de-bonding was successful with a variety of substrates: steel [24], aluminum [27], multi-material [25], and even fully composite joints (facilitated by stainless steel inserts) [28]. TEP-modified adhesives are generally desirable because they can be integrated into existing adhesive systems, limiting development time.

The use of TEP-modified structural adhesives for easy de-bonding presents some disadvantages, which include: (i) decreased thermomechanical stability (lower T_g), (ii) reduced joint strength and/or stiffness, (iii) lower peak operating temperature (below T_{start}), (iv) decrease in durability performance (higher moisture uptake), (v) adhesive

remnants on de-bonded substrates that may inhibit recyclability, and (vi) irreversible de-bonding. Furthermore, extra care must be taken during joint fabrication (e.g. in the mixing and cure processes) so as not to trigger premature particle expansion. Overall, TEP-modified adhesives can be integrated into existing adhesive systems for de-bonding on-command; however, they introduce issues in the manufacturing process (e.g. limited cure temperature, additional mixing steps for adding TEPs) and they can compromise bulk and joint properties.

1.3.2 Hot-melt adhesives

Hot-Melt Adhesives (HMAs) are thermoplastic polymer systems and they are generally not categorized as structural adhesives [19]. They are applied to a substrate in the molten state and allowed to cool below their melting point (T_m). The mechanical properties of HMAs are stable at ambient temperatures, and the de-bonding involves the re-melting of the adhesive; however, the melting temperature T_m of the crystalline portion limits their operating temperature range, with a very strict upper bound due to HMAs' rapid stress-relaxation rate. Furthermore, HMAs are not usually considered structural adhesives because of their relatively low LSS, with high performance HMAs typically showing a LSS between 2 and 4 MPa (considerably lower than the industry-standard 7 MPa for the "structural adhesive" classification) [19, 29]. Although a few published studies have demonstrated highly-engineered HMAs formulations with lap shear strengths as high as $\sim$18-23 MPa [30, 31], they generally have low thermomechanical stability and are mainly used in less critical environments (e.g. electrical components in computers). HMAs are re-processable, which offers the potential for re-bonding, but some permanent molecular damage occurs during reprocessing due to thermal degradation, and their recycling capability is therefore finite.

1.3.3 Nanoparticle additive-based de-bonding

Magnetically Active Nanoparticles (MNPs) are nanoparticles such as iron oxide (FeO_3) or manganese dioxide (MnO_2) that possess ferromagnetic, ferrimagnetic, superparamagnetic, or piezo-electric properties. These particles can be electromagnetically excited by alternating magnetic fields, resulting in induction heating (driven by eddy currents) [20, 32]. The nanoparticles are typically 1-100 nm in diameter, and they are typically added to adhesives by weight. At the particle-adhesive interface, MNPs that have been electromagnetically excited conduct heat to the adhesive layer, leading to adhesive softening and melting (when used in HMAs only). Cheng et Al. found that an HMA adhesive modified with 5 wt.% FeO_4 saw an increase in joint strength (7.4 MPa to 8.2 MPa) from the baseline, with further enrichment (up to 30 wt.%) causing a decrease in LSS [33]. Unlike TEPs, MNPs cannot be easily integrated into the majority of structural adhesives for de-bonding on command, because the de-bonding mechanism relies on the reprocessability of HMAs. MNPs can however assist the de-bonding of joints fabricated with low conductivity substrates like Fiber-Reinforced Plastic (FRP), by delivering induction heating directly to the adhesive layer, without having to rely on heat conduction from the substrate. Additionally, airborne MNPs emitted during joint fabrication pose potential threats to human health, with accidental inhalation or ingestion leading to respiratory diseases [34].

1.3.4 Electrochemically reactive adhesives (electrically-induced)

Electrically induced de-bonding relies on the modification of an adhesive system with salts. When the resulting ionically conductive adhesive is subjected to an applied electrical potential, electrochemical reactions occur at the adhesive/substrate interface, driving the adhesive's release (de-bonding). Electrochemically induced de-bonding is an established, commercially-available technology called ElectRelease™ [35]. This method

relies on the conductivity of the substrate and requires a proprietary conductive mesh insert as an alternative for non-conductive substrate materials.

1.4 Vitrimers

Covalent Adaptable Networks (CANs) are thermoset-derived polymeric materials with non-permanent cross-links [36, 37]. For CANs, the exchange reaction is categorized as dissociative or associative depending on the chemical reaction to elevated temperatures [38]. For dissociative CANs, cross-links are *reversible*. Added heat shifts the polymer's network toward depolymerization, whereby covalent bonds break and do not reform (i.e. de-crosslinking). Conversely, associative CANs are distinguished by *dynamic* cross-links that break and reform at equal rates, such that the total number of covalent cross-links remains constant and network integrity is maintained. Macroscopically, this results in heat-driven polymer flow, and broad reprocessability.

Associative CANs were first formulated in 2011 [39] and then called "vitrimers" in 2012 by Leibler et al. [40]. The term "dynamic covalent networks" has also been popularized in recent years. Vitrimers are synthesized with a base resin (often epoxy-based), curing agent(s), and internally or externally catalyzed to achieve a network with a heat-dependent bond-exchange rate. Bond exchange is often attributed to transesterification reactions. A vitrimer's bond-exchange rate, the rate at which the bonds break and reform, increases with temperature. The viscoelatic behavior of vitrimers exists in three regimes separated by two transition temperatures (see Figure 1.1), with the first being the glassy-to-rubbery transition (T_g) typical for polymeric materials. Above a secondary transition temperature, the "network topology freezing temperature", the bond exchange becomes so rapid that macroscopic plastic flow is induced. In the plastic flow regime, the material undergoes stress-relaxation and behaves as a viscoelastic liquid, which facilitates heat-driven topological rearrangement. Below the network topology

freezing temperature (T_v), the bond-exchange rate slows to a point where the network is essentially "frozen," and the material behaves as a typical thermoset. Due to their high strength and reprocessable nature, vitrimers offer a more sustainable alternative to traditional thermosets, with potential uses in self-healing, shape memory, and other recycling aspects.

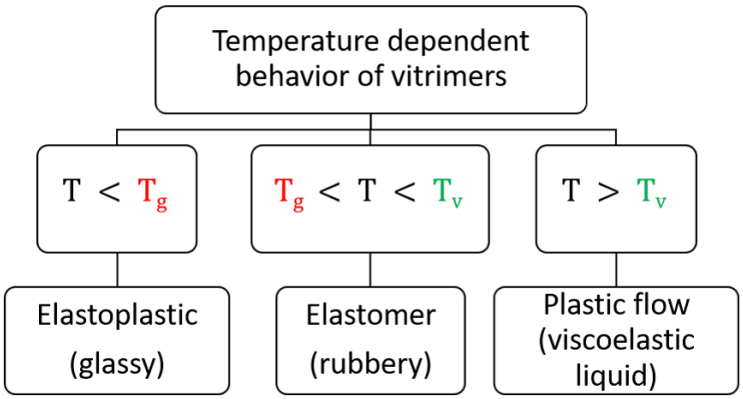

Figure 1.1: Viscoelastic behavior of vitrimers

In their work, Leibler et al. [39, 40] investigate a vitrimer based on a diglycidyl ether of Bisphenol A (DGEBA) resin, with a fatty acid curing agent (Pripol 1040), and an aqueous zinc solution ($Zn(ac)_2$) as catalyst. The bulk material performs as a thermoset under normal operating conditions — Modulus of Elasticity (E) $\sim$1.8 GPa, tensile strength (S_{ut}) $\sim$55 MPa. The cured network can be ground and recycled under heat and pressure (3 min at 240 °C) showing limited decrease in modulus and tensile strength when compared to the baseline bulk properties [39]. In their work, an important distinction is made between the thermomechanical stability of vitrimers versus thermoplastic polymers

[40]: (i) thermoplastics stress relaxation follows the Williams-Landel-Ferry (WLF) power law model for stress relaxation and (ii) vitrimers exhibit an Arrhenius-like model for stress-relaxation. Therefore, thermoplastic materials' stress relaxation is more rapid, which leads to limited applications.

Further rheological characterization of this first formulation is studied by Meng et al. [41], and a constitutive relation is determined, where transesterifications are the only rate-limiting reactions. Similarly to the Maxwell Model (Figure 1.2 [42]), the stress relaxation — and consequently the bond-exchange rate and effective viscosity — follows an Arrhenius-like relationship above the vitrimer's T_v, as shown in Figure 1.3:

$$\ln \tau = \frac{E_a}{RT} + \ln A \tag{1.1}$$

where τ is the characteristic relaxation time, E_a is the activation energy, R is the ideal gas constant (8.314 kJ/kmol.K) and A is the pre-exponential factor. The catalyst drives the transesterification reaction: therefore the bond-exchange rate and, consequently, the rheological characteristics can be easily tuned by varying the catalyst type and concentration [40].

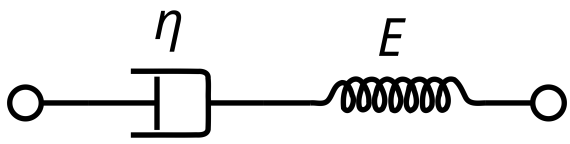

Figure 1.2: Maxwell model spring and dashpot representation [43]

In recent years, the pace of vitrimer research has accelerated, and mechanical and chemical recycling or reprocessing avenues of vitrimers have been explored. Chemical

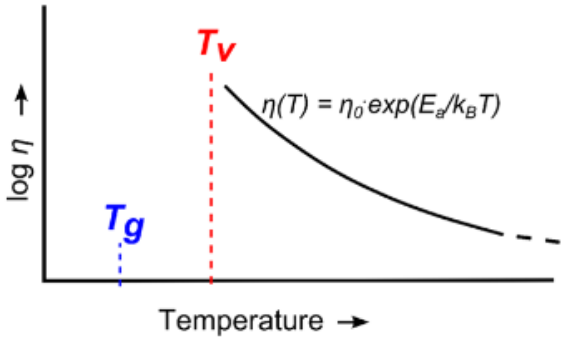

Figure 1.3: Representative graph of the Arrhenius-like temperature dependent viscosity of vitrimers above the network topology freezing temperature (T_v) [40]

recycling is particularly effective as a fiber reclamation technique for FRPs and can be done via solvolysis, pyrolysis, acid hydrolysis, etc. Mechanical recycling often involves mechanical grinding, heating, and compression molding with an autoclave or a hydraulic press with heated platens. The most common application for vitrimers is as matrix for fiber-reinforced composites, enabling fiber reclamation and self-healing [44, 45, 46, 47, 48]. Reprocessing of Carbon Fiber-Reinforced Plastics (CFRPs) is particularly attractive because of the high cost of the materials and manufacturing processes.

1.4.1 Vitrimers as adhesives

Associative CANs are a promising, but underexplored alternative method for controlled de-bonding. By taking advantage of its reprocessability in its stress-relaxed state, a vitrimeric adhesive can potentially be de-bonded, re-bonded, or welded. Recent preliminary studies investigate several bond-exchange reactions, other than transesterifications, such as disulfide exchange [49, 50], imine metathesis [51], quaternization reactions [52], and boron-nitrogen coordination [53]. The potential of

quaternization reactions is explored by Huang et al. [52], who developed an alkyne-azide-based vitrimer, called poly(1,2,3-triazolium) or VPTA, which was then used to bond Aluminum Alloy (AA) substrates. In this study, SLJs were fabricated by sandwiching and pressing a cured VPTA membrane between the substrates. The SLJs were then placed in an oven at 160, 180, or 200 °C for various time intervals, resulting in a LSS in the range of 7 to 26 MPa, depending on the processing parameters, upon first adhesion. Reassembly of the SLJ after destructive lap shear testing was highly effective, with LSS above 10 MPa (> 40% healing efficiency) for over 20 de-bond/re-bond attempts.

Among all of the available studies on vitrimeric adhesives, DGEBA (i.e. BADGE) is the most common monomer utilized as the "resin" in epoxy vitrimeric adhesive formulations. Several research works from the Universitat Rovira i Virgili by Santiago et al. [54], Surós et al. [55], Roig et al. [56], and Verdugo et al. [57] investigate the fitness of vitrimer materials as adhesives – the first three of which are BADGE-based epoxies and and the last being a bio-based vanillin. The studies regarding the BADGE-based epoxies investigate different curing agents and catalysts (Triazabicyclo[4.4.0]dec-5-ene (TBD) or 1-Methylimidazole (1MI)) of varying molar ratios towards an optimal formulation for bonding their prospective substrate material. Additionally, Roig et al. [56] demonstrate high self-healing potential for transesterification CANs in adhesively bonded joints, by calculating the healing efficiency on the baseline LSS (0.2 mm bondline thickness): (i) de-bonding and re-bonding (up to 63% healing efficiency), (ii) re-bonding after failure (up to 60% healing efficiency), and (iii) welding for first adhesion (up to 67% efficiency).

Some vitrimeric formulations rely on non-covalent interactions, such as hydrogen bonding or $\pi - \pi$ bonding, to maintain network integrity while still promoting topological rearrangement. In a study by Dong et al. [58] rigid-flexible integrated side chains with multiple interactions are introduced to a DGEBA resin matrix, with methylhexahydrophthalic anhydride (MHHPA) as the crosslinking agent, and catalyzed by

zinc nitrate hexahydrate (Zn^{2+}) in order to develop a vitrimer with excellent thermomechanical stability (T_g ∼129 °C) and good strength (LSS > 9 MPa), without compromising the bond-exchange rate. The resulting vitrimer network can be reprocessed in the stressed relaxed state (at 180 °C) or the material can be chemically degraded into oligomers (polymer intermediate with fewer repeating units) by submerging in tetrahydrofuran (THF) and H_2O, with triethanolamine (TEOA) as a catalyst at 50 °C.

Both reported bio-based vitrimer adhesives are developed with vanillin as the resin matrix and are internally catalyzed formulations, excluding the need for catalysts for bond-exchange. It is beneficial to forgo the need for catalysts as they are sometimes expensive and cause further risk of environmental damage, but more direct catalytic control of the bond-exchange reaction is forfeited with internally catalyzed formulations. As previously mentioned, a study by Santiago et al. [57] investigates bio-based vitrimers using Cystamine Bis(vanillin glycidyl ether) (Cyst-BVGE) as the epoxy resin which is synthesized from renewable vanillin and cured with four different imine crosslinking agents to create four unique vitrimer formulations. Formula tuning yields a vitrimeric adhesive with imine and disulfide groups which demonstrates fast relaxation times (∼2 s), T_g of 90 °C, T_v of 54 °C (notably below the T_g), and LSS up to 9.3 MPa. The novel material can be recycled by acid-assisted hydrolysis or heat-driven de-bonding, and re-bonding sees healing efficiency of up to 97%, but is affected by poor thermomechanical stability [57]. Similarly, Roig et al. [56] synthesize a bio-based vanillin vitrimeric adhesive with T_g up to 56 °C and LSS up to 12.7 MPa with mechanical recycling of bulk material via hot-pressing of powder (130 °C and 5 kPa for 2 h); chemical degradation is investigated through both acid hydrolysis and transamination.

Table 1.2 summarizes some of the results on vitrimer adhesive research from works published within the years 2017 to 2026. The source, resin, catalyst (if externally catalyzed), T_g and the collection method used, as well as the substrate material and

associated LSS are reported. The collection methods for T_g are either DMA or Digital Scanning Calorimetry (DSC). The substrates used in the studies for lap shear testing are either AA, steel, or stainless steel (SS).

Table 1.2: Properties of vitrimeric adhesive formulations from the current literature

Resin	**Catalyst**	T_g **[°C, Method]**	**LSS [Substrates, MPa]**	**Source**
VPTA (Alkyne-azide monomers)	–	92, DMA	AA, 7-25	[52]
DGEBA	TBD	64-81, DMA	DP 1000 (steel), 25.9-29.8	[54]
DGEBA	1MI	64-68, DMA	DP 1000 (steel), 26.6-27.5	[54]
DGEBA	1MI	66-80, DMA	AA 6060, 20.2-25.8	[55]
DGEBA	1MI	54-74, DMA	AA 6060, 10.1-16.1	[56]
Cyst-BVGE	–	90, DMA	DP 1200 (steel), 7.3	[57]
Bio-based Vanillin	–	26-56, DMA	AA 6060, 3.8-12.4	[59]
DGEBA	Zinc nitrate hexahydrate (Zn^{2+})	129, DMA	SS, 11.4; AA, 9.6	[58]
DGEBA	$Zn(ac)_2$	85, DSC	AA 6060, 9; SS 304, 9	[60]

As shown in Table 1.2, the lap shear strength of the vitrimeric adhesives ranges anywhere from 4 MPa to 30 MPa. Like typical structural resins, factors like the cure

schedule, surface preparation, substrate material, constituent ratios, and the catalyst are all contributors to the resulting properties. Besides the Cyst-BVGE bio-based vitrimer [57], the T_v typically lies somewhere above the T_g; therefore, a higher T_g often indicates a more stable network [40]. The T_g values for the reported vitrimeric adhesives are between 54 $^{\circ}$C and 129 $^{\circ}$C , which are comparable to commercially available epoxies.

Additional studies highlight the potential applications of vitrimers. Lee et al. [61] address the waste linked to EoL dismantlement of wind turbines by developing a disulfide reaction-based vitrimeric adhesive suitable for this application, with healing efficiency up to 70%.

1.5 Research gaps and objectives

Despite the recent surge in research on vitrimers and their application as structural adhesives, several fundamental aspects remain underexplored. First, it is unclear if the thermomechanical and environmental stability of vitrimer networks is comparable to traditional thermoset adhesives. Then, although most of the studies discussed in this Section measure the stress relaxation time at fixed temperatures, there is no direct reporting on time and temperature to de-bond for vitrimeric adhesives. Lastly, there is a lack of bulk material fracture toughness and creep performance data for CAN-based adhesives. Recently, several vitrimers have been developed for their use as composite infusion resins. Their formulations and curing process could be tuned to convert them to viable structural adhesives.

In this study, a vitrimer formulation comprised of diglycidyl 1,2-cyclohexanedicarboxylate (DCN) resin cross-linked with branched polyethylenimine (PEI) is proposed as a structural adhesive for aluminum substrates for reversible joints. Feng and Li [46], who introduced the DCN-PEI formulation, highlighted short processing times, a reasonable T_g, room temperature healing capability, and overall good mechanical

performance. The mildly cross-linked material is especially attractive because it is internally catalyzed by the PEI, disregarding the need for expensive catalyst and complex processing methods. The properties of DCN-PEI have been recently investigated by a separate research group: Tetteh et al. [62] studied its repeated impact strength and healing properties when used as composite matrix, while Mahoney, Tetteh, et al. [63] optimized time and temperature parameters for maximum healing efficiency. Building from these studies, this research aims to investigate the viability of DCN-PEI epoxy-imine vitrimer for structural adhesion. The performance of aluminum SLJs is assessed and improved to find the ideal permutation of constituent mix-ratio and cure schedule. De-bonding time and temperature data is collected during heat-induced de-bonding tests. The Mode I (opening) fracture toughness is investigated by preparing and testing double cantilever beam specimens. Environmental and thermal stability of the bulk material are measured using DMA of pristine vitrimer and after hot/wet cycling.

Similarly, the structural joining performance of a commercially available epoxy-imine vitrimer is investigated. The thermomechanical properties, mechanical performance, and healing capabilities are all experimentally tested. Results of the thermal characteristics are compared to the referenced studies. Details of adhesive and substrate materials, experimental methodology, and results are outlined, presented, and discussed.

CHAPTER TWO

MATERIALS SELECTION AND GEOMETRY OF TEST PARTS

In this chapter, the two tested vitrimer formulations, their source material, and the expected properties are described along with an explanation for the material choices. Joint substrate materials, test parts geometry, and test sample fabrication/manufacturing methods are also detailed.

2.1 Vitrimer formulations

Two vitrimer materials are investigated in this thesis: DCN-PEI (VA.1) is synthesized starting from its basic monomer constituents, and a commerically available epoxy-imine vitrimer (VA.2) is purchased. Both vitrimer formulations were previosly tested and used in their bulk form or as composite infusion resins.

The chosen resin and cross-linker for VA.1 are the monomers diglycidyl 1,2-cyclohexanedicarboxylate (DCN) and polyethylenimine (PEI), respectively. The DCN is purchased from Avantor (VWR) and has low viscosity. The branched PEI is purchased from Millipore Sigma, and has medium viscosity (800-5000 cP) and low molecular weight (average M_w $\sim$800, average M_n $\sim$600). The DCN-PEI vitrimer, first synthesized by Feng and Li [46], is chosen for its simple preparation process and commercially available constituents.

Following the synthesis route of VA.1 as shown in Figure 2.1, ring-opening polymerization of the epoxide form the DCN monomer. Covalent cross-links are formed by (i) the primary and secondary amines from the branched PEI, and (ii) the oxygen from the epoxides group creating ester linkages. The presence of dense hydrogen bonds between the oxygen of neighboring ester groups as well as between ester groups and primary amines provides VA.1 's unique capability for room temperature healing. The

mildly cross-linked vitrimer is internally catalyzed by the secondary and tertiary amines, allowing for dynamic ester exchange (i.e. transesterification) to occur at high temperatures.

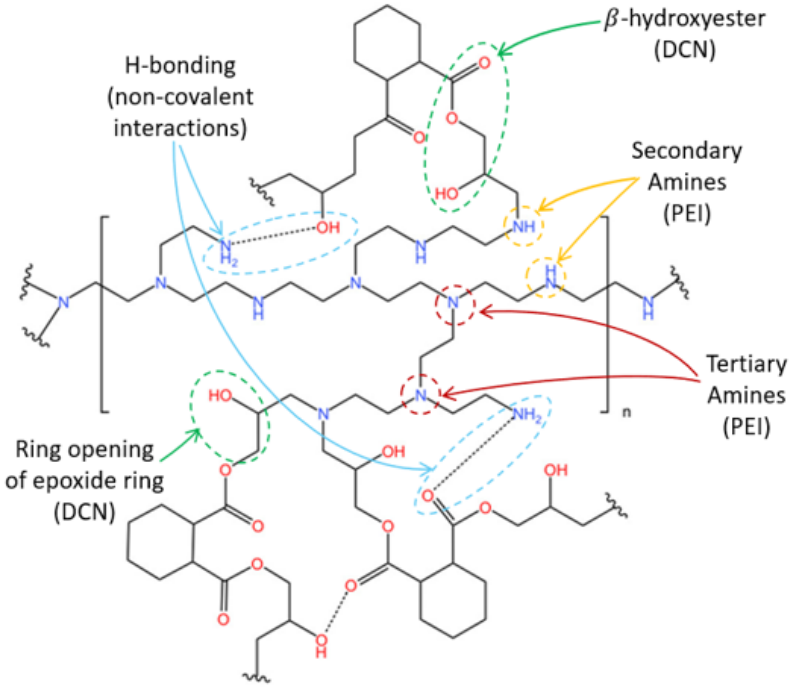

Figure 2.1: Synthesized DCN-PEI (VA.1) vitrimer (1:1 mass ratio) chemical structure, synthesis routes, and covalent and non-covalent bond reactions

2.2 Bulk material specimens

Bulk material specimens are molded in 4 different shapes, depending on test and equipment needs: discs, large rectangular samples, thin rectangular films, and dogbones. Disc-shaped bulk material samples are fabricated using a round silicone mold. The discs are 100 mm (4 in.) in diameter and approximately 2 mm (1/13 in.) thick (Figure 2.2).

Rectangular samples are used for dynamic mechanical characterization, and are cut from the prepared discs to the following dimensions: 12.7 mm (1/2 in.) width and 50 mm (2 in.) length. The sample thickness ranges from 1.59 mm (1/16 in.) to 2.54 mm (1/10 in.) with care taken to limit variation and decrease geometric factor effects. Smaller rectangular specimens are fabricated for tension film testing. The samples are sheared to size and are 35 mm (1.4 in.) long, 6.8 mm (.27 in.) wide, and 0.5 mm (0.02 in.) thick. Lastly, tensile test dogbones are fabricated following the ASTM D638 Type I standard [64]. The calibrated section is 13 mm (1.2 in.) wide, and the dogbones are 3.2 mm (1/8 in.) thick.

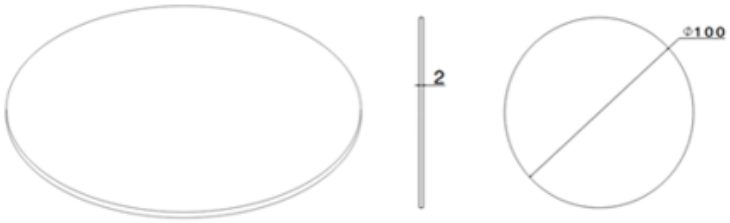

Figure 2.2: Disc geometry for bulk material samples (dimensions are in mm)

2.3 Joint specimens

2.3.1 Single lap joints

The chosen substrate material for the single-material single lap joints (SLJs) is rolled Aluminum Alloy (AA) 6061-T6 with a thickness of 1.6 mm (1/16 in.). Multi-material SLJs (with VA.2 adhesive) are fabricated bonding AA and CFRP substrates. CFRP adherends are the same thickness as AA substrates: 1.6 mm (1/16 in.). The CFRP adherends are made of 12K tow size carbon fibers arranged in a 2×2 twill

weave with a [0/90/0] stacking sequence in an epoxy matrix, and are purchased as cured panels. The material properties of the substrates are outlined in Table 2.1. The substrate materials are water-jet cut into 25.4 mm (1 in.) by 101.6 mm (4 in.) coupons with a 6.35 mm (1/4 in.) diameter hole on one end for the de-bonding test apparatus (Figure 2.3).

Table 2.1: Substrate material properties

Property	AA 6061-T6	CFRP
Young's Modulus (GPa)	68.9	32.5
Tensile Strength (MPa)	310	553
Elongation at Break (%)	12	1.7

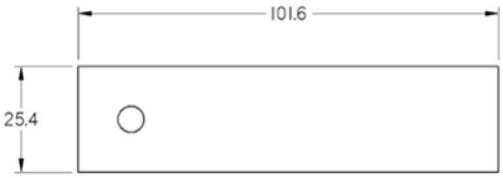

Figure 2.3: Coupon geometry (all dimensions are mm)

Joint specimens, like that in Figure 2.4, are fabricated with a 25.4 mm (1 in.) overlap length, for a total length of 177.8 mm (7 in.), and a nominal bond area of 645.2 mm^2 (1 $in.^2$). The adhesive layer is 0.12 ± 0.02 mm thick, and is controlled with an

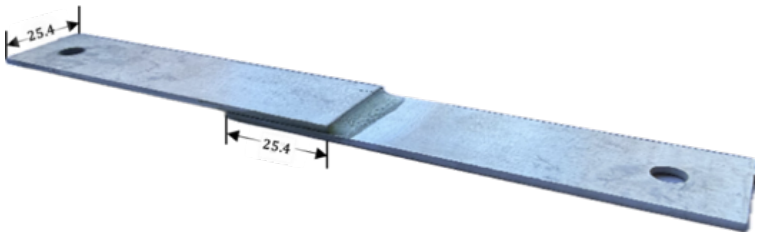

Figure 2.4: Single lap joint specimen (25.4 mm by 25.4 mm overlap area)

alignment fixture equipped with shims. The bond-line thickness is slightly lower than the ASTM D1002 standard [17] recommended 0.20 mm value. The low bond-line thickness is a compromise due to the relatively low working viscosity of the uncured vitrimer, which causes significant flow during manufacture and cure: a 0.12 mm-thick layer prevents excessive shrinkage and/or large voids. In real-life applications, the thickness of the adhesive layer is typically a fraction of a millimeter [65]. Bond-line thickness for adhesive testing is considered reasonable if it is within the range of 0.1 to 1.0 mm, with thinner ($\sim$0.2 mm) bondline thicknesses yielding higher shear strength than thicker ($\sim$1.0 mm) [66]. Although increased thickness typically leads to decreased strength, da Silva et al. [66] demonstrate that a small increase in thickness from 0.2 to 0.4 mm has insignificant impact on the overall joint performance. Similarly, the 0.12 mm bondline thickness is considered within the reasonable range for testing purposes. The fabricated joint specimens are used for lap shear testing, creep performance testing, and reversibility experiments.

2.3.2 Tapered (or contoured) double cantilever beam joints

There are two different geometries that can be used for joint fracture testing – flat adherend double cantilever beam or Tapered Double Cantilever Beam (TDCB). Mode I fracture toughness tests are performed using TDCBs, with AA 6061 adherends. During

Mode I fracture tests, the cantilever beam length increases as the crack opens, causing a drop in flexural rigidity when using flat adherends. Therefore, the calculation of opening mode fracture toughness (energy release rate) (G_{1c}) relies on the continuous measurement of crack length, which is very challenging especially with clear adhesives. To solve this issue, the geometry of TDCBs (Figure 2.5) is such that, as the crack opens, the flexural rigidity of the cantilever beams remains constant, eliminating the need for the continuous crack measurement. The specimens are water-jet cut from a 25.4 mm (1 in.) thick AA sheet. The height of the contoured edge is a function of the crack length and follows the relationship:

$$\frac{3a^2}{h^3} + \frac{1}{h} = m \tag{2.1}$$

where a is the crack length, h is the height, and m is a constant value (m = 90 as recommended by ASTM D3433 [67]). Polytetrafluoroethylene (PTFE) inserts are sheared from 0.2 mm thick shim-stock are used to create the initial crack and maintain the bond-line thickness during fabrication. PTFE is used due to its high temperature rating and low SFE for easy removal before testing. An initial crack length (a) of 25.4 mm (1 in.) is created using the PTFE inserts and is measured from the axis of the loading pin.

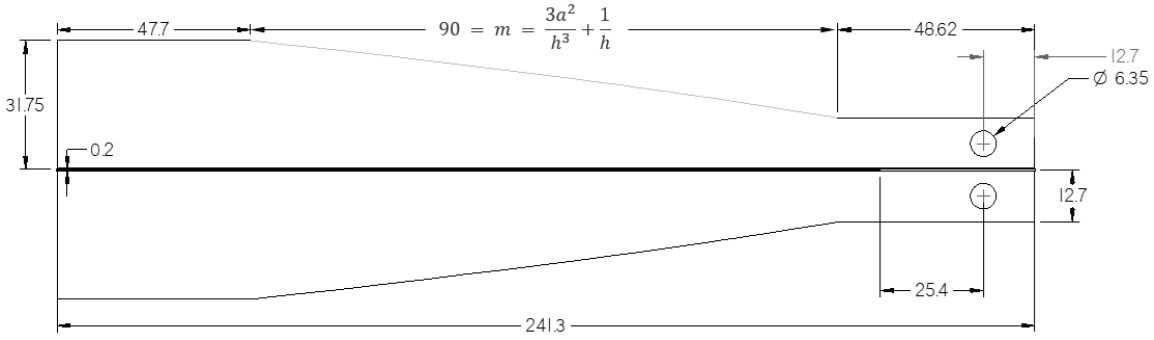

Figure 2.5: Contoured double cantilever beam specimen geometry [67]

CHAPTER THREE

EXPERIMENTAL SETUP AND METHODOLOGY

This section defines the fabrication steps for the bulk and joint test specimens including the vitrimer synthesis and cure procedure. Methodologies used for the bulk material characterization techniques and the assessing joint properties are also covered here.

3.1 Vitrimer formulation synthesis steps

3.1.1 DCN-PEI (VA.1)

Synthesis is a one-pot polycondensation of the monomers where the quantities are measured in non-stoichiometric mass ratios of DCN:PEI 1:1 or 2:1. The DCN monomer is transferred with a wide-tip pipette into a disposable polycarbonate cup followed by the PEI. The contents are thoroughly combined with a centrifugal mixer (AR-100 Thinky Planetary Centrifugal Mixer). The constituents are first mixed for 3 minutes and subsequently undergo a 1 minute-long de-foaming cycle to remove any entrapped air. The pot-life (i.e. the maximum working time) of the combined materials is 10 minutes. The material must also be synthesized in smaller quantities (typically 20 g per synthesis) as the critical mass is found to be at least as low as 50 g for the 1:1 mass ratio. Above the critical mass, rapid exothermic spontaneous cure occurs.

3.1.2 Commercial epoxy-imine vitrimer (VA.2)

For the second vitrimer formulation, the VA.2 is mixed in the recommended ratio of 1.5:1 imine resin hardener:epoxy resin. The imine hardener is heated to 80 °C for 2 h to reduce its viscosity for proper mixing. The epoxy is added first to the mixing cup, followed by the imine resin. The constituents are combined in the centrifugal mixture for

3 minutes, followed by a 1 minute-long de-foaming cycle to prevent air entrapment. The expected vitrimer properties are tabulated in Table 3.1.

Table 3.1: Commercial vitrimer (VA.2) expected physical properties

Physical properties	Value	Unit
T_g	80-180	°C
Moisture uptake	<1	wt.%
Viscosity (60 °C)	6,300	cP

3.2 Fabrication of test specimens

Before assembling the SLJs, the aluminum oxide layer at the bond surface area for the AA adherends is removed by mechanical abrasion with a steel wire brush drill attachment. Similarly, the surface of the CFRP bond area is lightly abraded by hand with 320-grit aluminum oxide sandpaper. The surface preparation is done to increase the SFE, which increases the level of intimate molecular contact and promotes adhesion [16]. Abrasion is also used to increase the surface roughness on a micro-scale and eliminate macroscopic unintended topography to improve mechanical interlocking and avoid curvature mismatching. The prepped aluminum coupons are cleaned and degreased in an ultrasonic acetone bath to remove any impurities (e.g. machine oils, weak oxides, or hydroxides) that may lead to a weak boundary layer (low SFE). Acetone can cause degradation to the polymer matrix, so the CFRP coupons are instead cleaned with SF1 biodegradable degreasing agent in the ultrasonic cleaner and allowed to air-dry thoroughly

before bonding. Once prepared, the adhesive is applied in an even layer to the bond area of each adherend with a bone cement spatula. The joints are assembled and cured in a custom alignment fixture. Calibrated shims are used to maintain appropriate bond-line thickness and the joints are subject to a constant pressure from the weight of a steel top-plate.

For VA.1, two cure schedules are used (Figure 3.1). The first tested cure schedule (CS1) involves a 2 h phase at 100 °C and a high temperature post-cure of 150 °C for 2 h. The CS1 curing schedule is obtained from the reference study [46]. A dark discoloration is observed from joints fabricated with the initial cure schedule (CS1). Therefore, a modified cure schedule (CS2) is introduced, with the high temperature post-cure removed. The overall dwell time is maintained to ensure the adhesive reaches full cure. Each of the four different VA.1 variations is a combination of the two mix ratios (1:1, 2:1) and two cure schedules (CS1, CS2). Three joints are fabricated and tested per variation. Cured specimens are stored under vacuum to prevent environmental aging.

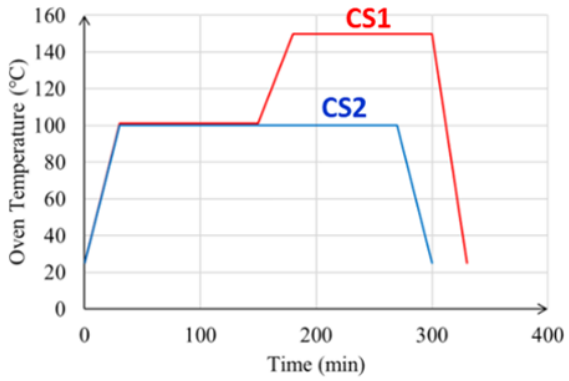

Figure 3.1: Cure schedule 1 (CS1) with 150°C high temperature post-cure and cure schedule 2 (CS2) with post-cure removed for DCN-PEI vitrimer (VA.1)

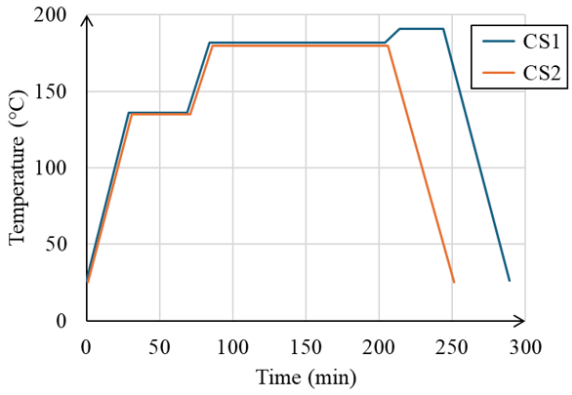

Figure 3.2: Cure schedule 1 (CS1) with 190°C high temperature post-cure and cure schedule 2 (CS2) with post-cure removed for VA.2

As with VA.1, two cure schedules (Figure 3.2) are used for the VA.2 formulation. The first cure schedule (CS1), recommended in the technical data sheet, uses a high temperature post-cure at 190 °C for 30 minutes. CS1 gives an expected T_g of 128 °C when VA.2 is used as a composite matrix. As with the VA.1-CS1, VA.2-CS1 exhibits a dark discoloration: the post-cure is therefore removed for the subsequent cure schedule (CS2). Two different substrate combinations are used with this formulation: fully aluminum (AA) and multi-material (MM) AA-CFRP joints. Four unique combinations are therefore tested: 2 substrate types with 2 cure schedules. The sample size is 3 joints per variation. The different SLJs and their nomenclature is given is Table 3.2.

3.3 Rheology characterization

3.3.1 Dynamic mechanical analysis

Dynamic Mechanical Analysis (DMA) is used to characterize the viscoelastic properties, such as the T_g, of a polymeric material. A cyclic strain excitation is applied to the polymeric sample, and the delay in the stress response is measured, as shown in the schematic in Figure 3.3. This method helps to determine the effect of changing the cure

Table 3.2: VA.1 and VA.2 SLJ nomenclature

Name	Epoxy:Imine Mix Ratio	Cure Schedule	Substrates
VA.1-1:1-CS1	1:1	CS1	AA
VA.1-1:1-CS2	1:1	CS2	AA
VA.1-2:1-CS1	1:1	CS1	AA
VA.1-2:1-CS2	1:1	CS2	AA
VA.2-AA-CS1	1.5:1	CS1	AA
VA.2-AA-CS2	1.5:1	CS2	AA
VA.2-MM-CS1	1.5:1	CS1	MM
VA.2-MM-CS2	1.5:1	CS2	MM

schedule, mix ratio, and moisture content on the viscoelastic properties and the estimated cross-linking density of the network. DMA of the VA.1 network is conducted with the TA Instruments Q800 dynamic mechanical analyzer in the 3-point bending fixture. Constant frequency mode is used at an amplitude of 15 μm and 5 Hz. The temperature ramp is 2-3 °C/min from room temperature ($\sim$24 °C) to 105 $\pm$ 25 °C, or at least 50 °C above the T_g; this is required to calculate the estimated cross-linking density (see Equation 3.1). T_g is taken as the peak of the tan(δ) curve.

Assuming the material follows the rubbery plateau, by using DMA and the storage modulus, the crosslink density (ρ_v) can be estimated by the following formula:

$$\rho_v = \frac{E'_r}{3RT} \tag{3.1}$$

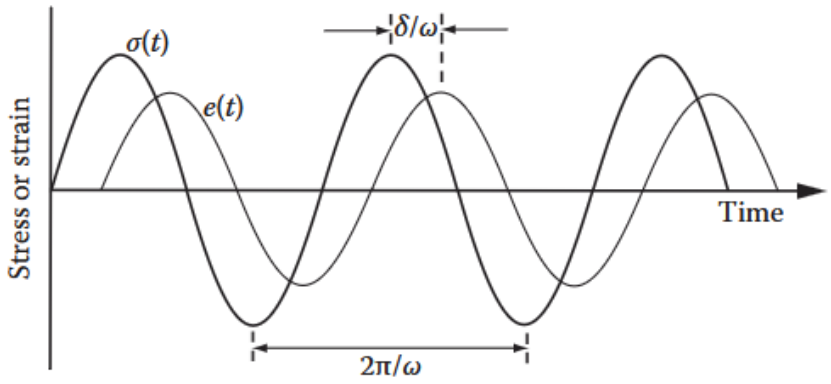

Figure 3.3: Phase angle obtained from sinusoidal applied stress at an angular frequency during DMA to determine tan(δ) [42]

where E'_r denotes the rubbery modulus, R is the ideal gas constant (8.314 m^3.Pa/K.mol) , and $T = T_g$ + 50 °C. Cross-link density can help to determine the effect of other parameters like thermal history or ratio of constituents on the structural integrity. A higher cross-link density is typically associated with high strength; however, too high a cross-link density may cause embrittlement and require plasticization to increase toughness.

3.3.2 Stress relaxation

Polymers are viscoelastic materials – they possess both viscous and elastic properties. When subject to a constant strain, viscoelastic materials undergo a time- and temperature-dependent decrease in stress response. This is referred to as stress-relaxation. In this study, stress relaxation experiments are used to determine the characteristic relaxation time (τ) by fitting the curve to the Arrhenius model (Equation 1.1).

Stress relaxation tests are performed with the TA Instruments DMA Q800, using tension film sample geometry. Samples are tested at temperature 125, 150, and 175 °C. Before the strain is applied, the samples first equilibrate at the test temperature for 30

minutes. During this first step, a small tensile preload (∼0.001-0.005 N) is applied to prevent buckling of the specimen due to thermal expansion. After equilibrating, a constant 2% strain is applied to the sample. The stress response of the material is recorded until the relaxation stress ($0.37\sigma_o$) is reached [42]. The data is fitted to the Arrhenius-like stress relaxation model to solve for the relaxation time.

3.4 Joint performance

3.4.1 Lap shear testing

Quasi-static lap shear tests are performed on the Hydraulic 810 Material Testing System (MTS) to investigate the joint performance of the vitrimer. A square area of 645.2 mm^2 (1 in^2) of each of the joint ends is clamped with tabs for proper joint alignment.

The joint specimen is pulled at a displacement rate of 12.7 mm/min (0.5 in/min) until failure. The corresponding force/displacement curves can be used to test and compare stiffness, ductility, and strength. The lap shear strength (LSS) is calculated as the peak load P_{max} normalized over the bond overlap area A:

$$LSS = \frac{P_{max}}{A} \tag{3.2}$$

The elongation at break d_u is the crosshead location at the maximum load. Three specimens per combination are tested and analyzed. The bond area fracture surface is also qualitatively analyzed for failure type – adhesive/interfacial or cohesive, with cohesive being the desired mode of failure.

3.4.2 Creep testing

Creep is the time-dependent strain response of a viscoelastic material subjected to a constant load below the material's yield strength. As observed in Figure 3.4, creep can be divided into 3 main stages: (i) primary creep (the initial strain response to the applied

load), (ii) secondary creep (stable and steady elongation over time), and (iii) tertiary creep (rapid, unstable elongation until failure). To characterize the vitrimeric adhesive's creep response at room temperature, SLJ specimens are tested at 10% , 25% , and 50% of the lap shear strength (P_{max} ∼10 kN for VA.1). The joints are tested for 20 h or until fracture.

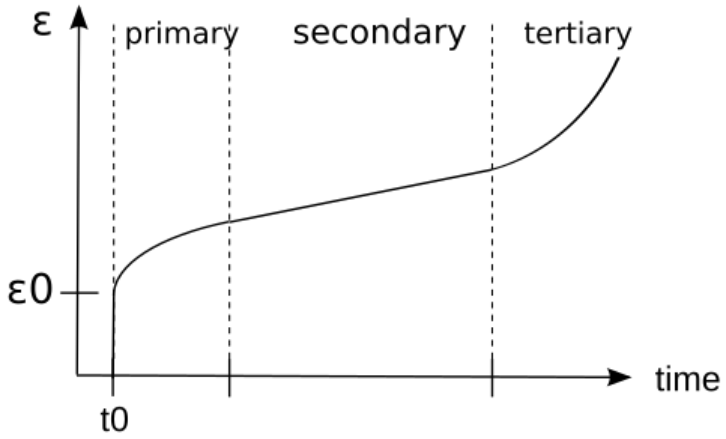

Figure 3.4: Stages of creep [68]

3.4.3 Mode I fracture toughness testing

Bulk material fracture can occur in 3 modes: Mode I (opening), Mode II (sliding), or Mode III (tearing) (Figure 3.5) [42]. As per the Standard Test Method for Fracture Strength in Cleavage of Adhesives in Bonded Metal Joints (ASTM D3433) [67], the resistance of a material to slow-stable or run-arrest fracturing under a severe tensile load is tested.

The Tapered Double Cantilever Beam (TDCB) specimen is mounted to the MTS via loading pins as shown in Figure 3.6. The cross-head displacement rate is chosen to be 1 mm/min, so that the test is completed in about 1 minute. When the crack begins to grow

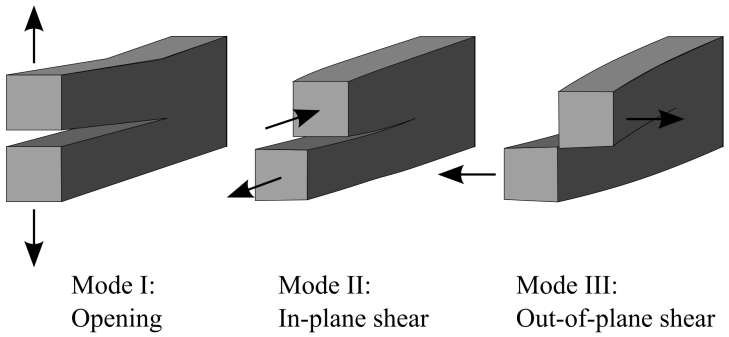

Figure 3.5: Fracture modes [69]

rapidly, the displacement is halted while the crack is allowed to continue growing. Once the response load from the test specimens stops decreasing, the load is reapplied until the appearance of a new uncontrolled crack growth. When the load has leveled off, the crack opening load (P_{max}) and the load when the crack stops propagating (P_{min}) are recorded. The steps are repeated up to 6 times or until uncontrolled crack propagation and failure.

Using this data, the two types of fracture toughness–opening mode crack critical toughness (critical energy release) G_{1c} and opening mode crack arrest toughness (energy release rate) (G_{1a})–can be calculated. The critical fracture toughness G_{1c} is calculated as follows:

$$G_{1c} = \frac{(4P_{max}^2)(m)}{EB^2} \tag{3.3}$$

where B is the specimen width, E is the tensile modulus of the adherend, and m is a constant value used to define the height at each crack length for contoured edge of the adherend (see Equation 2.1). The constant m is chosen as 90 in^{-1}, as it is a convenient value for adhesive testing and it is suggested by the ASTM standard [67]. Similar to Equation 3.3, the opening mode crack arrest toughness G_{1a} is:

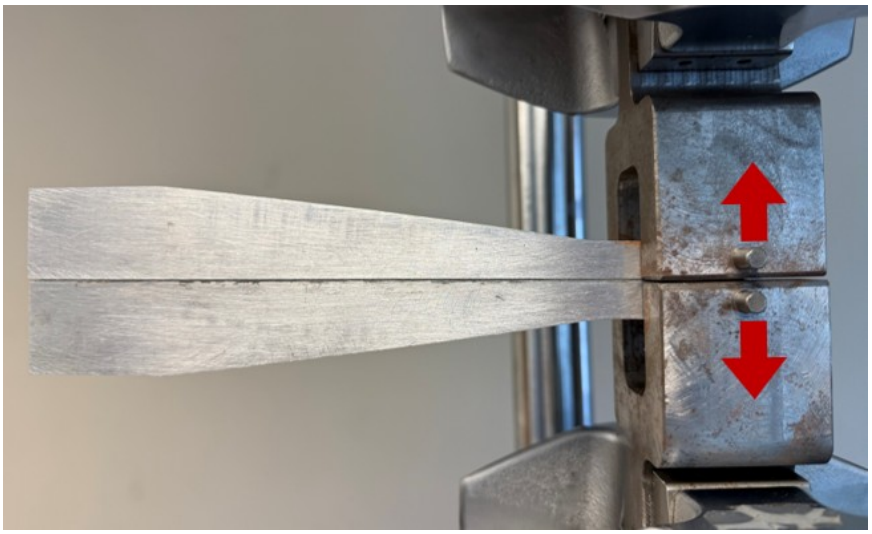

Figure 3.6: TDCB specimen in MTS grips

$$G_{1a} = \frac{(4P_{min}^2)(m)}{EB^2} \tag{3.4}$$

For these tests, TDCBs are fabricated and tested with the VA.1-1:1-CS2.

3.5 Durability

Polymeric materials are not impermeable to moisture. Therefore, it is highly important that the mechanical properties of a structural adhesive remain stable over its lifetime. Thus, their moisture uptake must be investigated. For an epoxy to be considered a viable structural adhesive, it must display reasonable environmental resistance, especially to water, which overall impacts its durability [19]. This is especially true when bonding materials that are more susceptible to corrosion, such as aluminum or FRPs, which can be accelerated by the presence of moisture [10].

Durability tests are performed on the VA.1 vitrimer formulation due to the hygroscopic nature of PEI. In fact, PEI is often utilized in the synthesis of cross-linked,

water-soluble polymers ideal for certain bio-medical applications like drug carriers. Moisture uptake is not investigated for the VA.2 because of the reportedly low moisture uptake ($< 1\%$) in the technical data sheet.

To measure the rate of moisture uptake, discs of the pristine VA.1 vitrimer are fully submerged in room temperature de-ionized (DI) water. The weight increase of the sample is measured at minute-long increments with a high precision scale (0.1 mg resolution) until peak saturation is reached. The moisture uptake of the discs is calculated as follows:

$$M_t(\%) = 100 \times \left(\frac{W - W_0}{W_0} \right) \tag{3.5}$$

where M_t is the percent weight of water at time t, W_0 is the initial weight of the sample, and W is the current weight. As a result of non-Fickian diffusion behavior for the room temperature submersion tests, true equilibrium is not reached and saturation is taken as the point when mass loss occurs [70]. Using this saturation value (M_∞), and assuming that the diffusion is Fickian in nature at least until $M_t = 0.5M_\infty$, the diffusion coefficient or diffusivity (D) of the material can be extracted using the following relationship:

$$D = \left(\frac{M_t \times h}{4M_\infty} \times \sqrt{\frac{\pi}{t}} \right)^2 \tag{3.6}$$

where h is the thickness of the specimen and t is the time. By this metric, the rate of moisture uptake can be more easily compared depending on temperature, concentration of moisture at the surface, and the synthesis parameters.

To further study durability of VA.1 and the effects of the thermal history on the thermomechanical properties, hot/wet testing of DMA specimens and DMA tests is performed. The cycled sample is subject to a 60 °C at 85% Relative Humidity (RH) for 24 h. The moisture uptake of the sample is recorded. Following the elevated temperature and

high humidity step, a drying step is employed for desorption of the specimen. The drying step is 50 °C and 5 % relative humidity. The dwell time is determined by the time it takes for the recorded mass to become relatively stable with respect to time ($\sim$ 72 h).

3.6 Reversibility assessment

3.6.1 Recovery of bulk properties

A rectangular DMA specimen that has undergone the hot/wet cycle outlined in section 3.5 is subsequently heated above the T_v. The healing temperature is chosen to be 140 °C based on the T_v reported by Feng and Li [46]. The sample is heated for 3 hours at this temperature and maintained at 0 % RH for 3 h. After the sample cools to room temperature, DMA is performed. The healing efficiency of the viscoelastic properties – Storage Modulus (E'), Loss Modulus (E"), T_g – as compared to the pristine DMA results are calculated.

3.6.2 De-bonding

De-bonding is the first reversibility step for vitrimeric adhesives. Heat-driven de-bonding of SLJs is performed via Induction Heating (IH). An induction coil is designed for this testing. The chosen coil design is a pancake (flat) coil due to the high efficiency of transverse flux heating for thin, flat workpieces. Moreover, the pancake coil heats the specimen from one side, thereby allowing unobstructed thermal imaging. Optimization of the number of turns (2, 2.5, or 3) and choice of square or round winding geometry is done by numerical modeling in Ansys Maxwell (Figure 3.7), where the configuration yielding the highest average Ohmic Loss (normalized over a 1 in.^{2} surface area) is chosen. To reduce edge effects that can occur from IH, preferred configurations include a coil diameter (or width) that is smaller than the bond area. The chosen coil design is a 2.5 turn, round coil.

Following the coil fabrication, RDO HFI 3.0 kW RF induction heating system is fitted with the custom 2.5 turn pancake copper induction coil. The coil is tuned depending on the tested vitrimer formulation (VA.1 or VA.2), cure schedule (CS1 or CS2), and the substrate materials (AA or MM). The resulting IH parameters are tabulated (Table 3.3). The de-bonding parameters are defined by the Current (I), Voltage (V), and frequency (f) associated with each coupled system. The actual power supplied (P) is approximated by the multiplication of the current and voltage (Equation 3.7).

$$P \approx V \times I \tag{3.7}$$

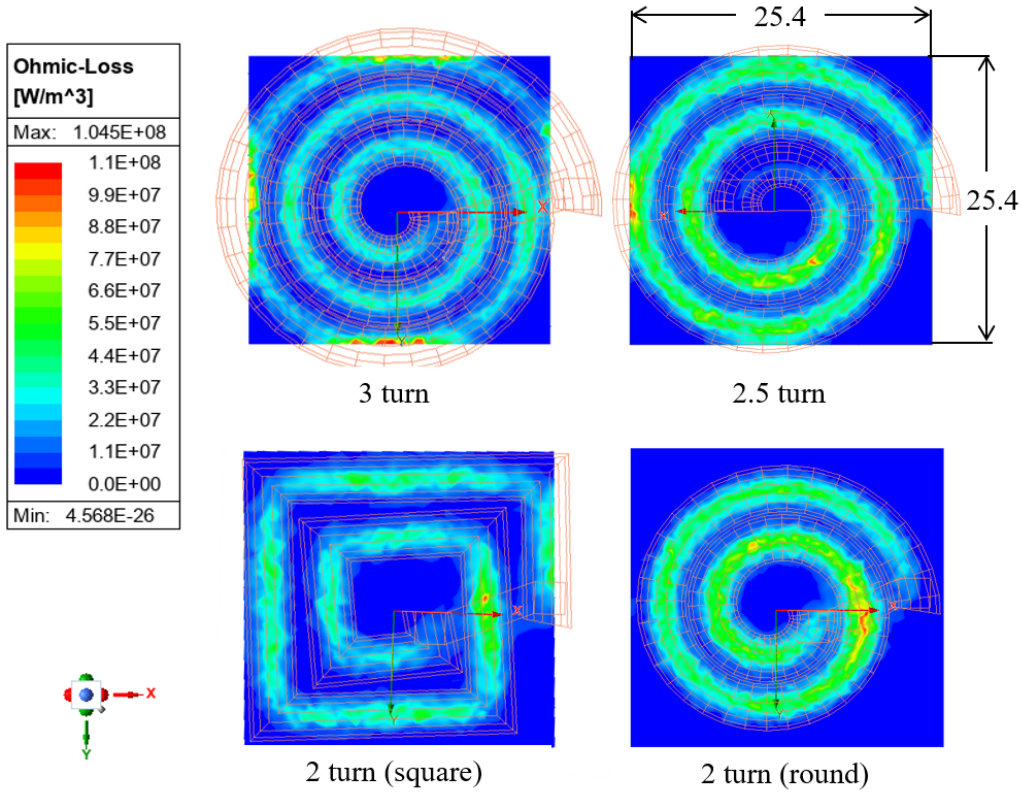

Figure 3.7: Visual comparison of Ohmic loss (W/m^3) based on the geometry of copper coil: 3 turn, 2.5 turn, 2 turn (square), and 2 turn (round)

Figure 3.8: De-bonding setup

Table 3.3: De-bonding test parameters depending on vitrimer formulation, monomer ratio, and cure for all CS2 vitrimer formulations

Parameter	**VA.1-1:1**	**VA.1-2:1**	**VA.2-AA**	**VA.2-MM**
Current (A)	52	51	53	57
Voltage (V)	39	36	43	51
Frequency (kHz)	155	157	155	148
Power (kW)	2.0	1.8	2.3	2.9

During de-bonding tests, a relatively small load of 100 N (∼20 lb.) – chosen to be less than 1% of the average LSS – is statically applied with a string/pulley system (Figure 3.8) to one end of the joint while the other end is pinned to the fixture. The substrate is heated by IH and heat is then conducted from the aluminum to the vitrimeric adhesive layer, to raise the temperature above the network topology freezing temperature (T_v).

Single lap joint specimens for VA.1-1:1-CS2, VA.1-2:1-CS2, VA.2-AA-CS2, and VA.2-MM-CS2 undergo de-bonding tests. Using a custom-built XY camera gantry and an infrared (IR) camera (FLIR A50 thermal camera), the temperature of the top surface of the substrate at the time of de-bonding is collected. Figure 3.9 shows the top surface of the joint where the IR camera collects the thermal images during the de-bonding tests. Before the de-bonding tests are performed, the joints are coated in a matte black, ceramic coating with a high temperature rating. This is to imitate a black body with a high emissivity (ε ∼0.94) for a more accurate temperature reading. The average temperature over the bond area as well as the visual temperature distribution are collected.

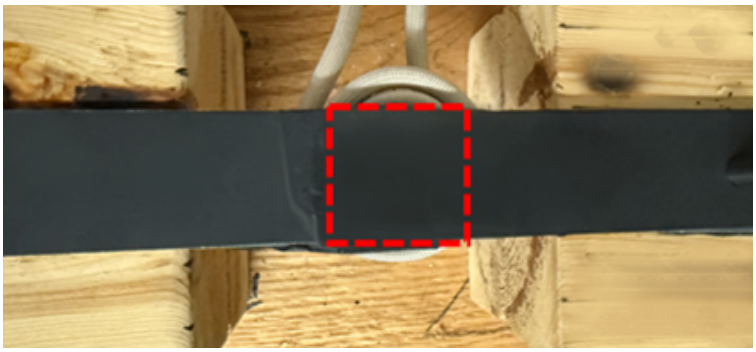

Figure 3.9: Thermal imaging camera view

3.6.3 Re-bonding and self-welding

To further determine the reversibility performance of vitrimeric adhesives, joints are assembled using 2 different processes: re-bonding and self-welding. In both cases, a layer of cured adhesive is present on each substrate prior to joint fabrication. Both assessment types attempt to harness the vitrimer flow characteristics by applying pressure at an elevated temperature to bond area. The formulations chosen for welding performance testing are the same as the de-bonding – VA.1-1:1-CS2 and VA.2-AA-CS2.

As shown in Figure 3.10, welding is performed using a KP-3, 5-ton (5T) table-top hydraulic press with dual heated platens (T_{max} = 149 °C). The weld process is controlled by the weld parameters – actual pressure, plate temperature, and time under load (i.e. dwell time). The actual pressure is calculated using the ratio of area of the hydraulic cylinder to the area that the force is applied. Since the bond area is 1 in^2, the actual pressure estimate is obtained by simply multiplying the area of the cylinder (1.43 in^2) by the hydraulic pressure. The weld parameters differ between the tested vitrimer formulations. One VA.1-1:1-CS2 self-weld (SW) sample is tested and no VA.1-1:1-CS2 re-bonding (RB) specimens are tested. The VA.1 weld sample is pressed at 7.5 MPa actual pressure with two heating steps – 80 °C for 3 hours + 100 °C for 30 minutes. Five VA.2-AA-CS2 SW specimens and 2 VA.2-AA-CS2 RB specimens are tested using the welding parameters given in Table 3.4.

To maintain accurate SLJ alignment without interfering with the stress distribution over the bond area, a fixture that is thinner than the bonded cross-section is utilized. To prepare a joint for welding, the adhesive overflow is removed from the substrate edges. Then, the substrates are fitted into the fixture and placed in the press. Before pressure is applied to the joint, the platens are heated to the weld temperature. Once that temperature is achieved, the hydraulic pressure is sandwiched between the platens at the

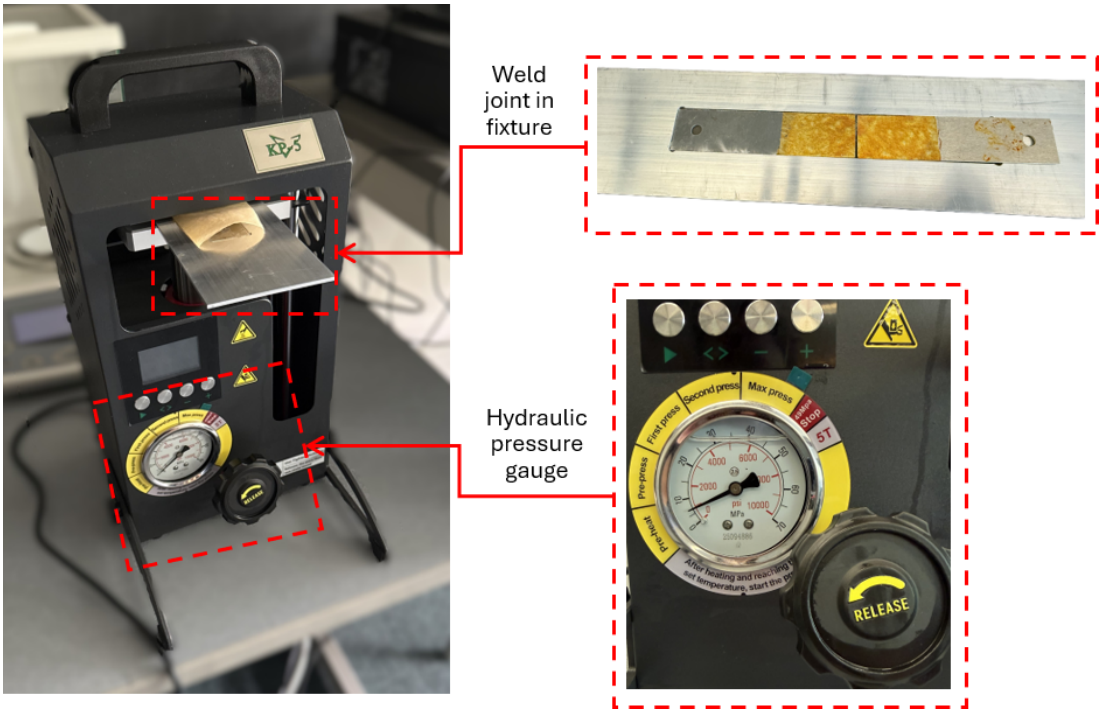

Figure 3.10: KP-3 Hydraulic press with weld sample, "open-face" self-weld sample in alignment fixture, and pressure gauge

pre-determined pressure. The pressure is reapplied every 30 minutes until the dwell time is reached, to account for pressure drops associated with the stress relaxation of the material. Finally, the pressure is decreased to 1 MPa, and the welded joint is left in the press until it cools to ambient temperature. This is done to avoid any joint separation from the pressure release in the stress-relaxed state.

Conversely, re-bonded (RB) sample fabrication and testing is a multi-step process. First, the SLJs are fabricated and cured as per typical fabrication (Sec. 3.4.1). Then, the joint undergoes controlled de-bonding via induction heating, as described in Section 3.6.2. The de-bonded specimens are allowed to cool, but are promptly pressed once they reach ambient temperature to avoid contamination of the adhesive layer.

Table 3.4: Weld parameters for VA.2-CS2 (commerical epoxy-imine vitrimer) SLJs

Weld Type No.	**Dwell Time (min)**	**Plate Temp. (°C)**	**Pressure (MPa)**
W1	10	100	10
W2	30	100	10
W3	60	100	10
W4	60	120	10

The self-welding (SW) specimens mostly differ from the re-bonded specimens in the initial fabrication steps. Unlike the re-bonded specimens, the self-weld substrates are fabricated unconventionally in an "open-face" configuration. As seen by the VA.2 SW sample in Figure 3.10, the bond areas of the substrates are coated and cured separately. After the substrates are created, the welding process follows the same steps as the re-bond testing.

Recent studies employ convection heating and solvent-based methods for vitrimeric adhesive joint reprocessing, and perform joint re-bonding after lap shear failure [54, 55]. Given the high strength of the formulations used in this thesis, re-bonding after lap shear failure is not attempted: lap shear tests result in significant yielding and permanent curvature of the aluminum substrates. The resulting curvature mismatch of the two yielded substrates would prevent intimate contact of the two bond areas during re-bonding.

CHAPTER FOUR

RESULTS AND DISCUSSION

Material characterization results – bulk tensile strength, dynamic mechanical analysis, stress-relaxation, and durability assessment – are presented for both DCN-PEI (VA.1) and the commercial vitrimer formulation (VA.2), organized by mix ratio and cure schedule. In addition, joint characterization results for VA.1 (AA only) and VA.2 (AA and MM) – lap shear tests, creep analysis, Mode I fracture toughness (critical energy release rate), and reversibility performance (de-bonding, re-bonding, and welding) – are discussed in this chapter.

4.1 DCN-PEI (VA.1)

This section summarizes and discusses the results from both the bulk and joint (AA only) characterization experiments for the DCN-PEI vitrimer formulation (VA.1). DMA is performed on all VA.1 variations. However, additional bulk material characterization is performed specifically on VA.1-1:1-CS2 (1:1 mix ratio, removed high temperature post-cure phase), because of its excellent joint performance.

4.1.1 Tensile properties

For VA.1-1:1-CS2 only, 2 different displacement rates (1 and 100 mm/min) are tested. Polymers are viscoelastic materials, therefore their mechanical properties are strain rate-dependent. As expected, higher displacement rate yields higher strength (S_{ut} = 29 MPa) and lower strain at break (ε = 0.05). Lower displacement rate leads to higher elongation at break (ε = 0.35), lower tensile strength (S_{ut} = 11 MPa), and greater energy absorption [42]. Lower strain rates allow for the polymer chains to re-align in the direction of the applied load [42].

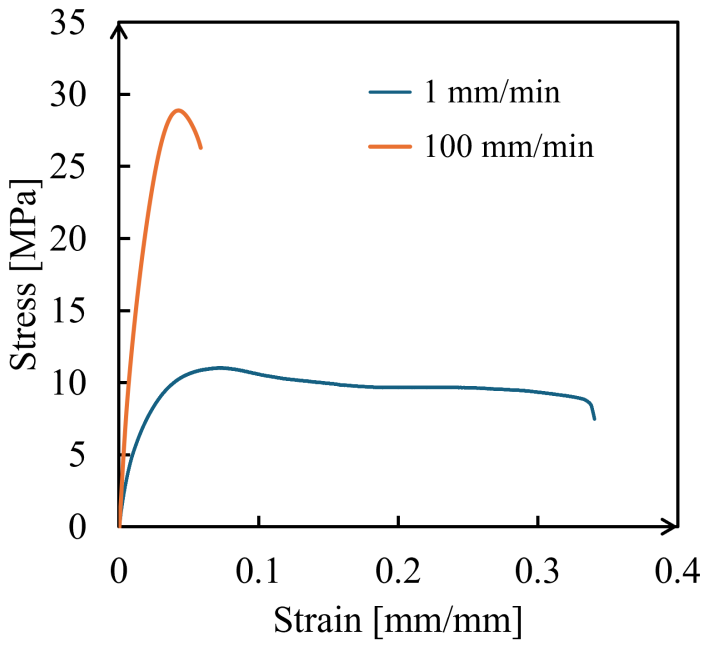

Figure 4.1: Engineering stress-strain curve for VA.1-1:1-CS2 ASTM D638 Type I dogbones subject to tensile load at 1 mm/min and 100 mm/min displacement rates

4.1.2 Viscoelastic properties

For DCN-PEI, the first tested cure schedule (CS1), is obtained from the literature and uses a high temperature post-cure. Higher temperature cure typically results in higher cross-linking density and improved strength of the bulk material [19]. Likely, the aluminum substrates and steel alignment fixture are conducting heat directly to the thin adhesive layer during cure which causes the vitrimer to cure at a faster rate as compared to a typical curing process in a mold.

The T_g for 1:1, CS1 is 59 °C lower than the T_g (DMA) from Feng and Li [46] of 72 °C. Notably, the T_g is lower than in the reference study, despite using a higher DMA frequency of 5 Hz (as compared to 1 Hz used by Feng and Li), which is typically associated with higher measured T_g values [71]. The tested value – despite the significant

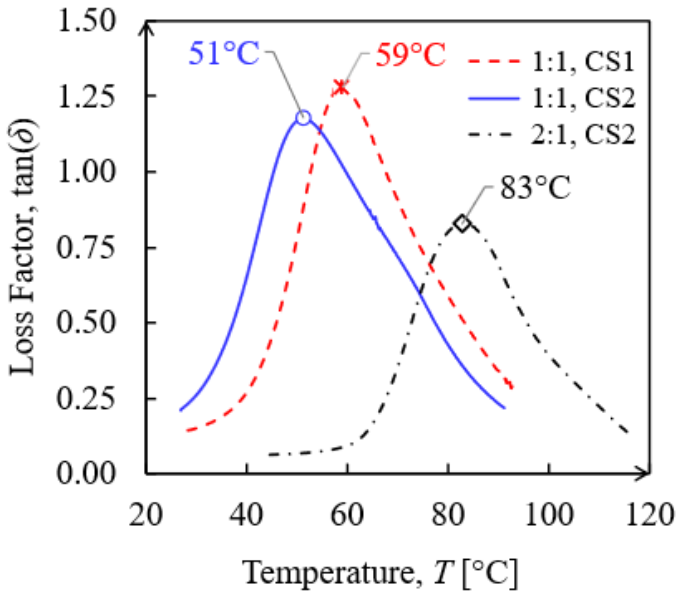

Figure 4.2: The tan(δ) curves of VA.1-1:1 (CS1 and CS2) and VA.1-2:1 (CS2 only)

discrepancy with the literature – is accepted because it falls between the values obtained from DSC (41 °C) and from DMA (72 °C) in the reference study [46]. The VA.1-1:1-CS1 DMA yields a rubbery modulus of 11.21 MPa. Similarly, there is a discrepancy from the rubbery modulus at T_g + 50 (T = 122 °C), which Feng and Li [46] report to be 3.5 MPa.

Higher T_g is symptomatic of a greater cross-link density from the higher cure temperature, as exhibited by the 8 °C decrease from CS1 to CS2 for the 1:1 ratio. Similarly, the effect of the mix ratio from 1:1 to 2:1 for the CS2 yields a higher T_g of 83 °C. The higher concentration of the DCN resin in the 2:1, CS2 combination suggests that a larger number of ester groups is present, leading to an overall increase in covalent cross-linking, while being closer to the stoichiometric ratio than the 1:1 ratio. The higher T_g for the 2:1 monomer ratio aligns with the trend observed in the reference study [46].

4.1.3 Stress relaxation

Stress relaxation tests are carried out for VA.1-1:1-CS2 samples. The resulting stress-relaxation times from 125 to 175 °C range from 1.5 h to 9 min, respectively. The inverse relationship relaxation time and temperature is expected for the positive Arrhenius-like relationship. The resulting data is presented in Figure 4.3. The fast relaxation time at 175 °C ($\tau \sim 9$ min) is similar to the value obtained from the major reference study. The relationship obtained from the Arrhenius model relaxation time can be used to infer the recycling temperature [46].

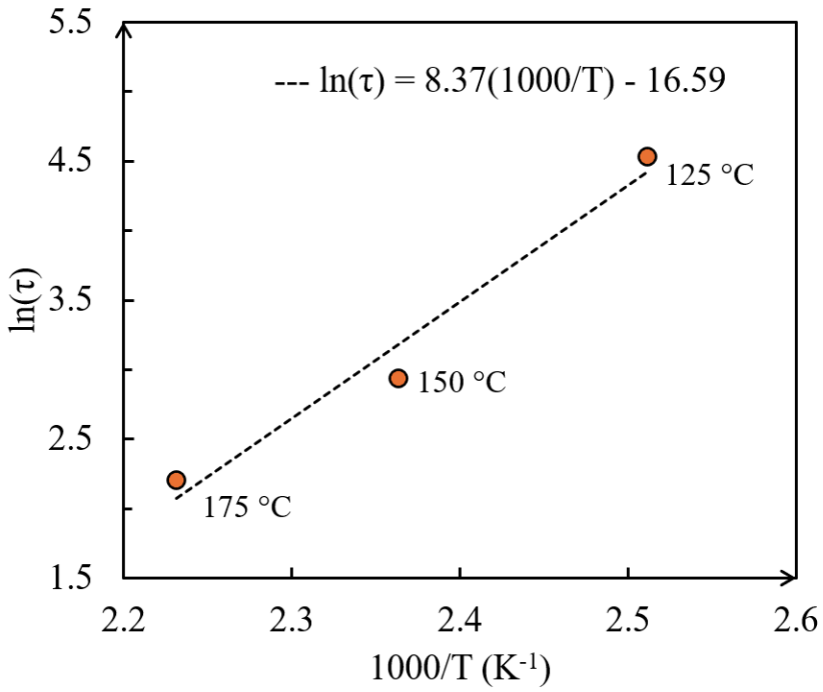

Figure 4.3: VA.1-1:1-CS1 $\ln(\tau)$ vs. 1000/T (K^{-1}) data for 125, 150, and 175 °C . The dashed line is the linear fit to the data points.

By fitting the natural log of the relaxation time $\ln(\tau)$ vs $1000/T$ with a linear model, the activation energy (E_a) and pre-exponential factor (A) can be determined. From the relation, E_a is found to be 69.5 kJ/mol. This value is smaller than what is reported in the literature (E_a = 98 kJ/mol) [46]). It is likely that the lower activation energy is a result of the lower-temperature cure schedule and its effect on the vitrimer's viscoelastic properties (E', T_g, and ρ_c).

4.1.4 Durability

Submersion tests are used to determine the moisture uptake of the material at room temperature. Even at room temperature, bulk material samples lose significant stiffness within 14 days in non-controlled humidity environments. Submersion testing is performed for both 1:1 and 2:1 mix ratios (both CS2) to determine peak saturation (M_∞) and rate of diffusion (D). The slope from the linear fit of the moisture uptake vs. root time data ($M_t \times h \,/\sqrt{t}$) in Figure 4.4 is substituted into Equation 3.6 along with M_∞ to determine room temperature D. Table 4.1 summarizes the bulk characteristics of VA.1-1:1-CS2 and VA.1-2:1-CS2: D, M_∞, T_g, Rubbery Modulus (E'_r), and ρ_v.

Figure 4.4 and the results listed in Table 4.1 show the high rate of moisture uptake of VA.1-1:1-CS2 and VA.1-2:1-CS2. Although diffusion is rapid for both samples, the rate of absorption of VA.1-1:1-CS2 is more than 3 times higher than that of VA.1-2:1-CS2. This is likely due to the 2:1 ratio being closer to the stoichiometric ratio, which lends itself to a decreased amount of polar groups (less H-bonding) on the molecular level, and, in turn, is likely responsible for the lower diffusivity coefficient. Further validation comes from the higher estimated cross-linking density of the 2:1 ratio (Table 4.1) and consequent tighter packing of the chains [72]. Overall, the VA.1- 1:1-CS2 and VA.1-2:1-CS2 moisture uptake and rate of diffusion are both high as compared to conventional epoxies — typically, $M_\infty < 3\%$ and $D \sim$1.0E-13 m^2/s [73]. As a result, rate

of diffusion of VA.1-1:1-CS2 and VA.1-2:1-CS2 is 2 orders of magnitude higher than typical epoxies [74].

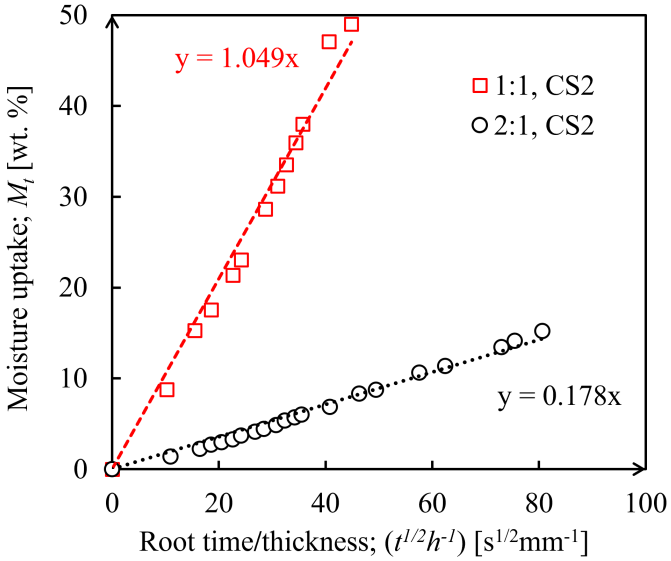

Figure 4.4: The room temperature moisture uptake M_t by percent weight vs. root time over thickness of DCN-PEI 1:1 (VA.1-1:1-CS2) and 2:1 (VA.1-2:1-CS2) for the optimal cure schedule

Table 4.1: DCN-PEI viscoelastic properties and durability summary

Mix ratio & cure	M_∞ **[wt.%]**	D **[m^2/s]**	T_g **[°C]**	E'_r **[MPa]**	ρ_v **[mol/m^3]**
VA.1-1:1- CS2	49	9.0E-11	52	11.2	1.2E+3
VA.1-2:1-CS2	15	2.7E-11	83	33.5	3.3E+3

To the author's knowledge, none of the studies investigating the DCN-PEI vitrimer report the extremely high rate of moisture uptake of the synthesized material. The major reference [46] demonstrated some swelling but overall excellent stability of VA.1 in many solvents (e.g. acetone, hexane, toluene, etc.), but the high presence of polar groups makes the network especially vulnerable to moisture absorption. Although it is limited, there is some evidence of humidity control due to the hydrophillic nature in the existing literature: Feng and Li [46] mention that the vitrimer was kept in a vacuum desiccator between testing and the study optimizing healing efficiency mentions the use of a nitrogen environment to remove moisture after strength tests and before welding [63]. As a result, this study considers optimal healing conditions only and does not account for the likely environmental effects. A high rate of diffusion is also observed in a study with a different imine-derived CAN formulation that found that "water-plasticization" could be advantageous for recycling purposes: the shift towards hydrolysis was minimal and stress-relaxation was possible at lower temperatures [73].

The effects of water plasticization are typically reversible upon drying. However, the mass loss that is observed during moisture uptake analysis indicates the possibility of crazing, hydrolysis, or chain scission – all of which are irreversible processes that degrade mechanical properties. To examine permanent impact of the high rate of moisture uptake on the network's properties, DMA results of pristine and cycled/dried samples are compared. During tests, it is qualitatively observed that the VA.1 bulk material becomes rubber-like, tacky, and drastically loses stiffness. Notably, the moisture uptake of the sample at an elevated temperature is higher than that of the fully submerged samples. After 24 hours at 85% RH and 60 °C, M_t reached 72 wt.%. This value is 23% higher than when mass loss occurred for the discs submerged at room temperature. Similar studies of the water absorption of epoxies report that Fickian diffusion occurs at temperatures above T_g and non-Fickian diffusion below T_g [75].

Figure 4.5 shows 2 VA.1-1:1-CS2 DMA samples held under different environmental conditions. The sample on the left is a pristine sample (i.e. a sample that has not undergone hot/wet cycling), whereas the sample on the right is shown after hot/wet and drying steps. There is a clear visual difference between the two samples, with the cycled vitrimer showing a dark discoloration as compared to the pristine sample. Discoloration of epoxies is typically caused by thermal oxidation. However, in this case the discoloration is likely exacerbated by the high temperature at which moisture uptake occurs.

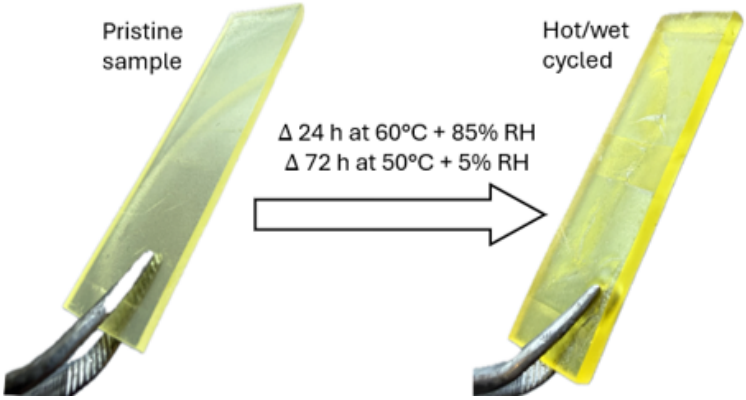

Figure 4.5: Rectangular DMA specimens of pristine VA.1 1:1 vitrimer (left) and after hot-wet cycling (right)

The thermal effects could be significantly contributing to the softening that occurs above T_g. When the vitrimer is within the rubbery region, the chains are further apart and the network is less rigid. Although there is likely negligible chain movement, hydrogen bonds are also more susceptible to temperature effects.

The drying cycle continues until the mass of the sample is constant over time (i.e. the mass reaches steady-state). This steady mass occurs after approximately 72 hours in the thermal chamber at 50 °C and 5% RH. No mass loss was observed; however, not all of the moisture was able to be desorbed under these conditions, and the final moisture uptake is recorded as 9.4 wt.% (higher than a typical structural adhesive). Figure 4.6 shows the DMA test results before and after the hot/wet and drying cycle.

4.1.5 Joint lap shear strength

The lap shear strength of the vitrimer combinations is determined via conventional SLJ lap shear tests. As seen in Figure 4.7, VA.1-1:1-CS2 outperforms the other three sample sets in both LSS and elongation. The strength of the VA.1-1:1-CS2 joints is comparable to the performance of typical structural adhesives. The effect of the cure cycle on joint performance differs depending on the mix ratio: for the 1:1 monomer ratio, higher ductility is observed upon the removal of the high temperature cure (CS2), with an ultimate elongation d_u (1.1 mm) 3 times larger than that of CS1 samples (0.3 mm). As a result, the strength of VA.1-1:1-CS2 joints is higher than that of the VA.1-1:1-CS1 despite the lower viscoelastic properties of the bulk materials, as softer/more flexible adhesives typically perform better under lap shear conditions. The opposite effect is seen for the 2:1 ratio, where both joints show brittle failure, and the average strength and elongation decreases from CS1 to CS2. This suggests that the performance of joints that suffer from brittle failure are governed by the cross-link density.

The variance in the elongation for all permutations is large, with the VA.1-1:1-CS2 joints having the largest relative standard deviation (RSD) of 46%. The large variance is attributed to different non tightly-controlled environmental conditions during the synthesis process. This is especially important given the reported instability of the VA.1 formulation in humid environments.

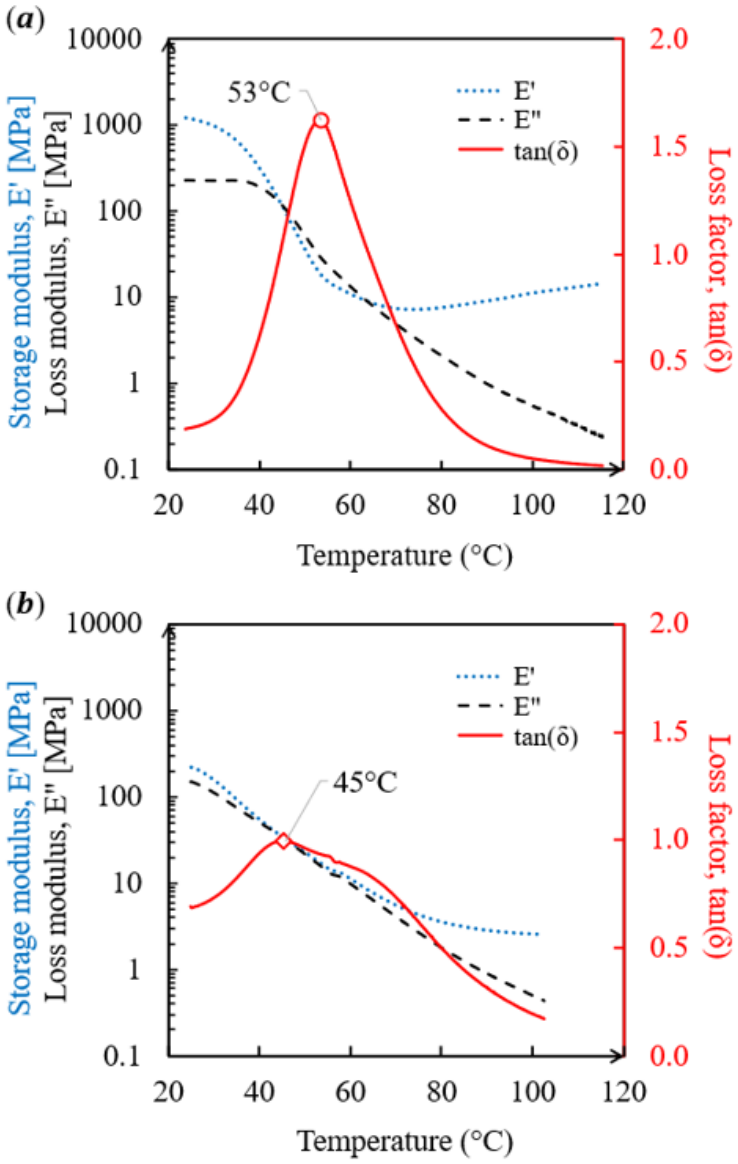

Figure 4.6: Moisture uptake of DCN-PEI 1:1, CS2 from hot/wet testing impact on DMA

Toughness is an important characteristic in structural adhesives. Higher bulk viscoelastic moduli do not typically guarantee higher joint strength: strong, stiff, but brittle adhesives can fail at relatively low loads at the substrate/adhesive interface (interfacial or adhesive failure). Unmodified structural epoxy adhesives have low

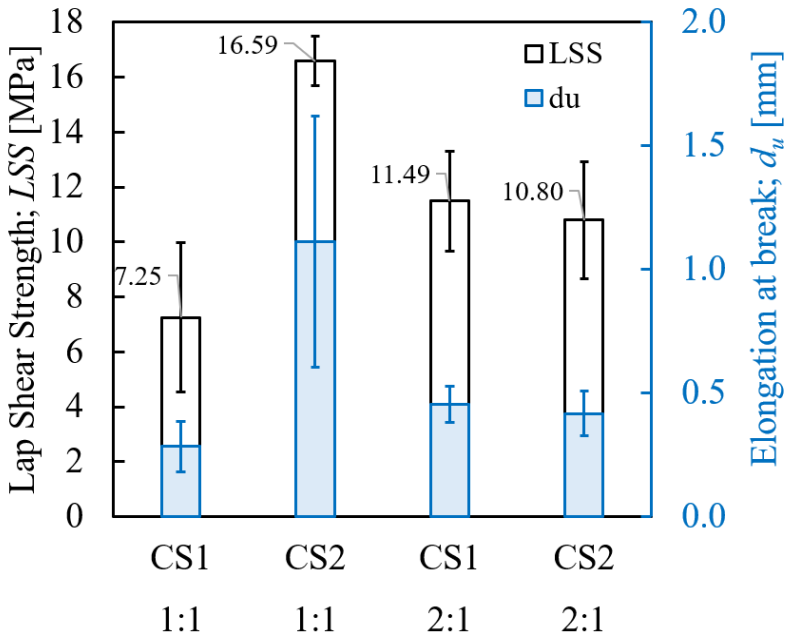

Figure 4.7: DCN-PEI (VA.1) lap shear test summary (error = 1σ)

toughness (~0.1-0.5 kJ/m^2) and low elongation at break, which hinders energy absorption within the bond-line. VA.1-1:1-CS2 joints show both high strength and toughness.

4.1.6 Joint creep performance

Due to the lower relative strength and brittle failure of the other mix ratio/cure schedule combinations, the creep and fracture toughness experiments are tested on the VA.1-1:1-CS2 variation only. Data for elongation vs. time under load for VA.1-1:1-CS2 SLJ creep experiments is shown in Figure 4.8. The joint subjected to a creep loading equal to 10% of the LSS does not fail within the allotted 20 h test period and remains within the secondary creep stage. The maximum elongation is less that 0.05 mm under the applied load. At the higher ratios (25% and 50%), the joints undergo all three stages of creep and fail before the allotted 20 h loading period.

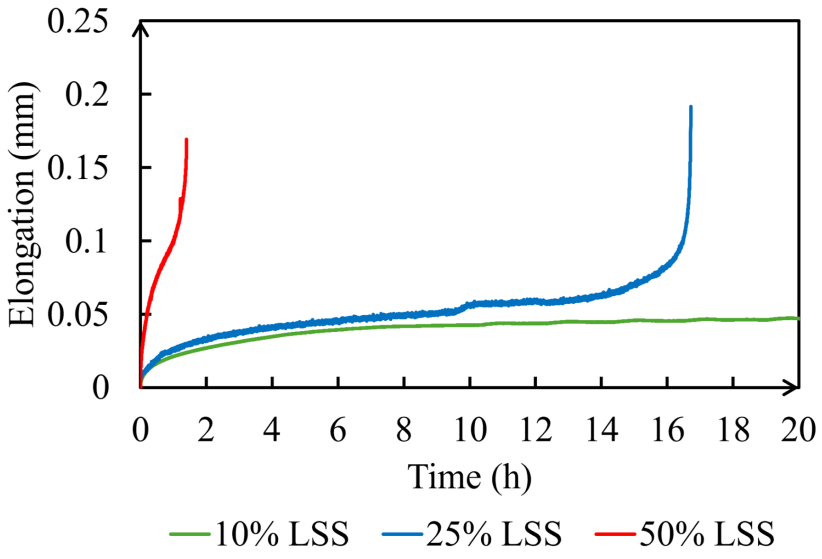

Figure 4.8: DCN-PEI (VA.1) creep test elongation vs. time curve at 10% , 25%, and 50% of the lap shear strength

4.1.7 Mode I fracture toughness

Mode I fracture toughness results are shown in Figure 4.9. The force-displacement curve shows that the TDCB specimen undergoes 1 initial crack propagation and 1 crack arrest recovery before uncontrolled crack propagation leads to joint failure. The resulting P_{max} is 2.4 kN and the P_{min} is 2.0 kN. These values, highlighted in Figure 4.9, are substituted into Equation 3.3 and Equation 3.4 to solve for Mode I fracture toughness (G_{1c}) and the crack arrest toughness (G_{1a}).

The G_{1c} is 1,819 J/m^2 and the G_{1a} is 1,360 J/m^2. These values are comparable to typical toughened epoxy adhesives. However, because only one test was performed, similar variance as seen in the LSS results could appear in fracture toughness test data. Therefore, further testing is required to assess the statistical variance in G_{1c} and G_{1a} values.

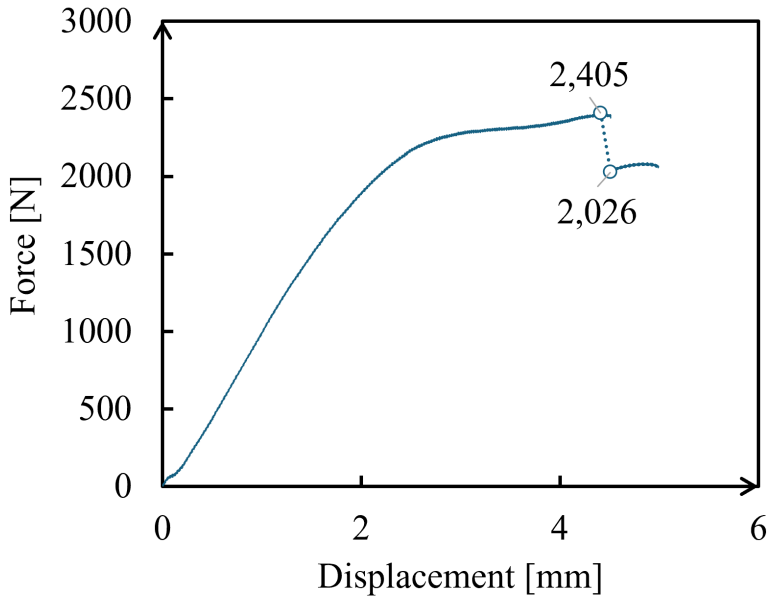

Figure 4.9: DCN-PEI (VA.1) fracture toughness (displacement rate = 1 mm/min)

4.1.8 Reversibility

Reversibility assessment consists of de-bonding and self-welding tests. De-bonding results for both VA.1-1:1-CS2 and VA.1-2:1-CS2 are reported. Preliminary assessment is performed on one representative specimen for the self-welding of VA.1-1:1-CS2.

The results of the de-bonding tests are summarized in Table 4.2. De-bonding of VA.1-1:1-CS2 is successful for samples with a $t_{de\text{-}bond}$ of 141 ± 34 s at the prescribed 100 N (20 lb) load. The average surface temperature at the time of de-bonding is 211 °C (± 2% accuracy) (Figure 4.10). VA.1-2:1-CS2 samples take over 2 times longer to de-bond (298 ± 119 s) than 1:1 monomer ratio samples; however, much larger variance is observed. As expected, the de-bonding temperature ($T_{de\text{-}bond}$) is also higher for

VA.1-2:1-CS2. The higher values for $t_{de\text{-}bond}$ and $T_{de\text{-}bond}$ are in line with the T_g values and cross-link density values obtained from the bulk characterization of VA.1.

Table 4.2: VA.1 de-bonding performance dependent on cure schedule (* indicates there there was only 1 representative sample)

Formulation	$t_{de\text{-}bond}$ **(s)**	$T_{de\text{-}bond}$ **(°C)**
VA.1-1:1-CS2	143 ($\pm$ 35)	211 *
VA.1-2:1-CS2	298 ($\pm$ 119)	247

The minimum collected temperature on the VA.1- 1:1-CS2 SLJ bond area top substrate surface is above 150 °C. This is important because the literature reports the T_v to be 134 °C or 150 °C (depending on the source), with 150 °C as the accepted value for the optimal recycling temperature. As seen in Figure 4.11, the temperature is not evenly distributed across the surface area and is instead concentrated to one side. This is likely due to both the geometry of the coil and the off-centered bond area in the de-bonding apparatus. Future de-bonding tests will be performed with care to center the bond area for better temperature distribution to optimize de-bonding efficiency.

Some VA.1-2:1-CS2 samples showed a very dark discoloration that could be attributed to thermal degradation. This is especially present in the samples which took longer to de-bond. Therefore, the de-bonding of the VA.1-2:1-CS2 SLJs may not be attributed solely to chain movement, but also to some thermal degradation of the joint. The $T_{de\text{-}bond}$ at 247 °C for VA.1-2:1-CS2 is marginally higher than the desired value for de-bonding at low loads.

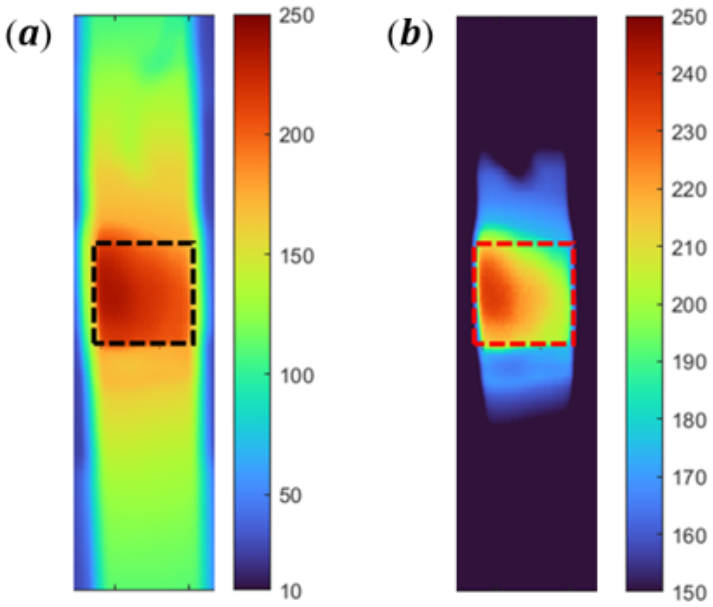

Figure 4.10: IR images of the same surface area of a VA.1-1:1-CS2 SLJ just before de-bonding on two different colormap scales: (a) 10 °C to 250 °C and (b) 150 °C to 250 °C

Welding is limited to one representative sample for the VA.1-1:1-CS2 due to the environmental instability of this formulation, which is accelerated by the high temperature at which both de-bonding and re-bonding/welding occur. The welded joint yields a 20 % (3.23 MPa) healing efficiency, calculated on the the initial average LSS of 16.59 MPa (Table 4.3). Despite the observed low healing efficiency, these results prove that the healing properties of the VA.1 material can be harnessed to fabricate re-bondable joints. Further optimization of the weld parameters should be pursued, to attempt to approach the high *bulk material* healing efficiency reported for 1:1 monomer ratio (84% [46]) and for 3:1 monomer ratio (51% [63]). Furthermore, the welding capability of the VA.1 formulation further validates the vitrimeric behavior of the material.

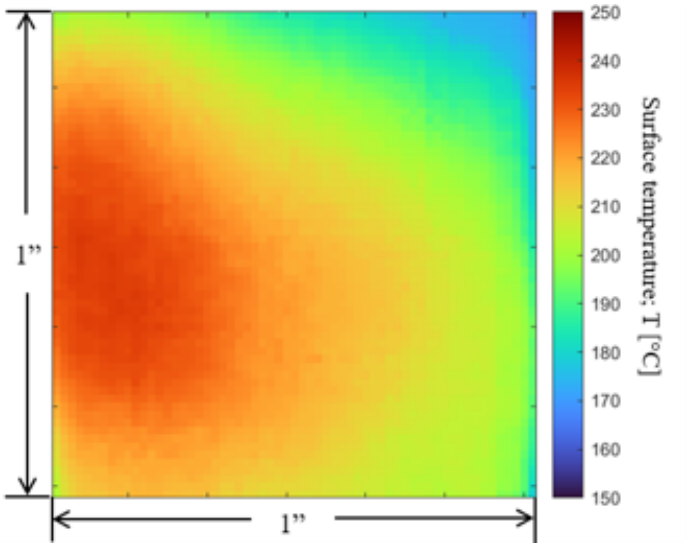

Figure 4.11: Top substrate bond overlap area surface temperature (°C) of VA.1-1:1-CS2 at time of debonding

Table 4.3: VA.1 welding strength recovery summary

Formulation	Baseline LSS (MPa)	Re-bond LSS (MPa)	Self-welding LSS (MPa)
DCN-PEI-1:1-CS2	16.59	-	3.23 (20%)

4.2 Commercial Epoxy:Imine Vitrimer (VA.2)

4.2.1 Viscoelastic properties

Bulk characterization is performed for VA.2 material to assess the impact of the recommended high temperature post-cure. This differs from the VA.1 analysis as there is only one monomer ratio tested (1:1.5 Epoxy:Imine ratio). The bulk viscoelastic properties of the vitrimer are not reported in the literature, so the results are compared to the 128 °C T_g from the FRP's technical datasheet. The T_g calculated for CS1 is 101 °C – lower than

the T_g given in the technical datasheet. Upon the removal of the 195 °C post-cure for CS2, the T_g drops to 87 °C. The resulting viscoelastic properties are summarized in Table 4.4.

Table 4.4: VA.2 formulations' viscoelastic properties summary

Mix ratio & cure	T_g **[°C]**	E'_r **[MPa]**	ρ_v **[mol/m^3]**
VA.2-CS1	101	48.8	4.6E+3
VA.2-CS2	87	15.2	1.5E+3

As shown in Figure 4.12, a distinct secondary transition is visible in the $\tan(\delta)$ curve, at 137 °C (CS1) and 109 °C (CS2). This large secondary transition could indicate inhomogeneity in the polymer blend. Further analysis of the polymer blend and the possible phase separation of the constituents is a necessary next step. Using the DMA results, the cross-link density is estimated for both cure schedules. The higher cure temperature in CS1 yields a 200% increase in cross-link density when compared to CS2 samples. This trend is also observed for the VA.1 formulation.

4.2.2 Joint lap shear strength

Fully aluminum (AA) and mixed-material (MM, AA-CFRP) SLJs are tested. The resulting joint strength and elongation at break are reported for both configurations, and for CS1 and CS2 curing schedules. As seen in Figure 4.13, the lap shear strength is highest for VA.2-AA-CS1 (i.e. VA.2 aluminum SLJs with post-cure), which also shows low variance. As for the MM joints, CS2 yields a strength of 17.01 MPa, which is higher than the 16.13 MPa average for CS1. As with the VA.1 joint performance, the increase in

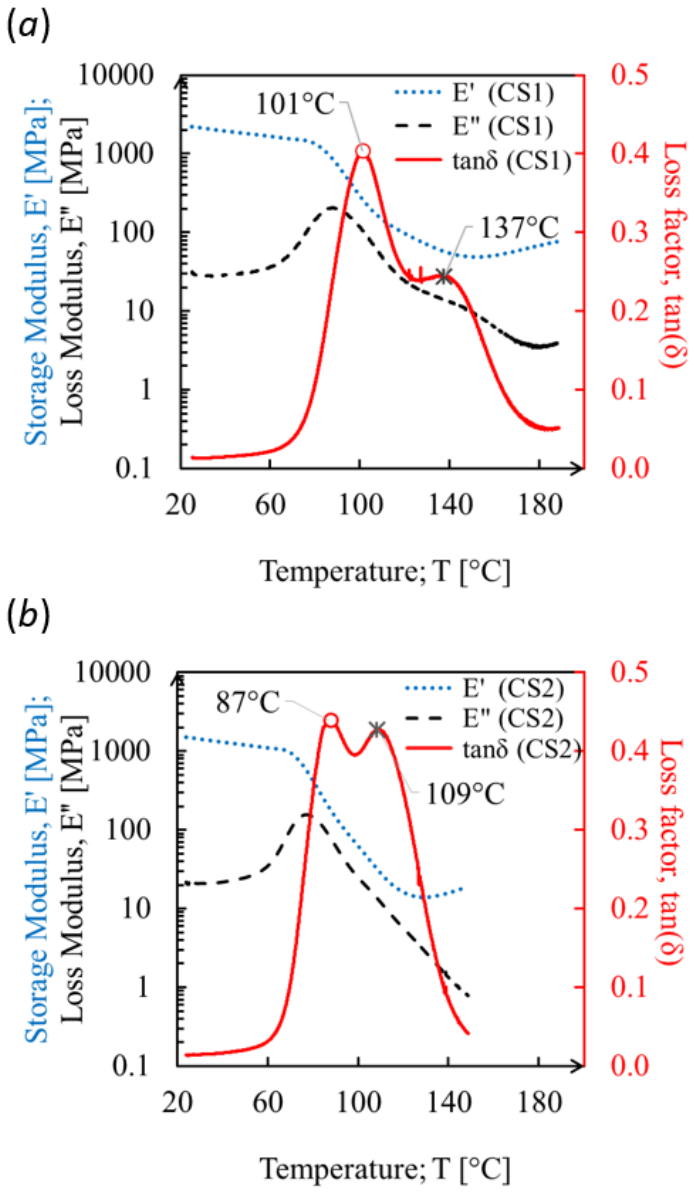

Figure 4.12: VA.2 DMA results depending on cure schedule: (*a*) CS1 (with high temperature post-cure) and (*b*) CS2 (removal of post-cure)

cure temperature leads to a decrease in joint ductility. However, in this case, since ductile failure is also observed in VA.2-AA-CS1 joints, the presence of a high-temperature post-cure phase (CS1) yields to higher lap shear strength. The consistent ductile failure

also leads to lower standard deviation in LSS data for all joint types. The elongation at break for the CS2 is higher for both SLJ types.

For both cure schedules, a decrease in LSS is observed when transitioning from single material to multi-material joints. This trend is reflected in the available literature [25]. CS1 samples show an 11% decrease in LSS and a 43% decrease in average elongation at break when comparing AA to MM joints. This trend is observed in CS2 data as well, with a 5% decrease in joint strength and 52% decrease in elongation at break. For both cure schedules, the CFRP substrate in the mixed-material joints causes a notable decrease in joint ductility, with a small impact on the joint strength.

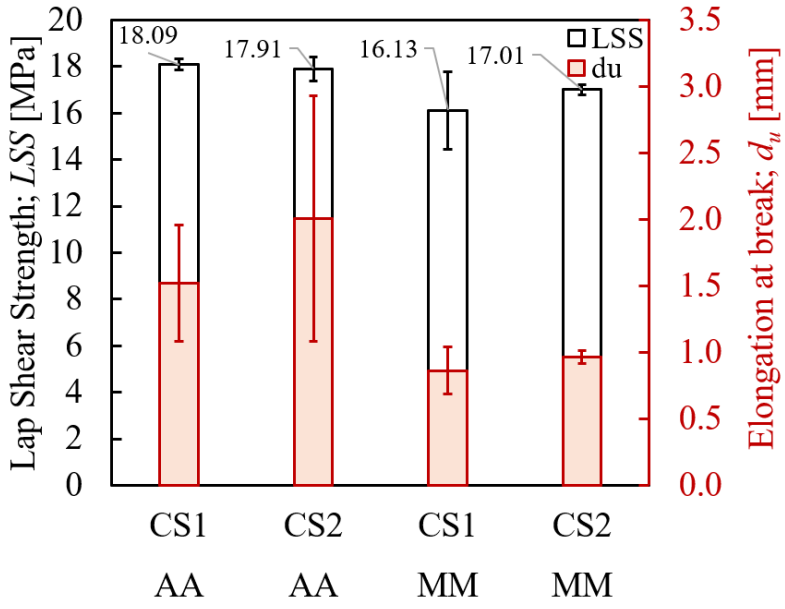

Figure 4.13: Commercial Epoxy:Imine vitimer formulation (VA.2) lap shear strength assessment summary (error = 1σ)

4.2.3 Reversibility

VA.2-AA-CS2 and VA.2-MM-CS2 joint de-bonding tests are performed, with all tested samples de-bonding successfully. The average $t_{de\text{-}bond}$ is 170 $\pm$ 28 s, as listed in Table 4.5. The de-bonding time for the tested MM joint is faster than the time for AA joints, at 146 s. This could be due to the heating technique: the joint is heated via IH of the aluminum substrate (on 1 side only in MM joints), which then heats the adhesive layer via conduction. CFRP's low through-thickness (i.e. normal to the woven fibers) conductivity [76] traps the heat within the bond-line, thereby increasing the heating rate and, consequently, the de-bonding efficiency. The fast de-bonding time shows that vitrimeric adhesives may be used to de-bond multi-material joints for substrate recovery. However, future studies should capture the de-bonding temperature of the CFRP substrate material, as high temperatures may lead to thermal degradation of polymeric matrix.

Table 4.5: VA.2 de-bonding performance dependent substrate materials (* indicates there there was only 1 representative test)

Formulation	$t_{de\text{-}bond}$ **(s)**
VA.2-AA-CS2	170 ($\pm$ 28)
VA.2-MM-CS2	146 *

Using the weld parameters given in Table 3.4, self-welding (Self-Welding (SW)) is performed for VA.2-AA-CS2 joints only. The results are summarized in Table 4.6. The W4 welding parameters set (Table 3.4) result in the highest LSS. The healing efficiency for re-bonded (Re-bonding (RB)) SLJs is as high as 53%, with an average of 48%. For

SW SLJs, the healing efficiency is as high as 47%, with an average of 45%. The lower strength seen in the SW specimens is likely due to the topological mismatch of the "open-face" substrates: the adhesive layer displays a significant curvature, due to the high surface tension of the vitrimer prior to "open-face" cure. Adhesive surface sanding may help to correct the topological mismatch and increase contact area for improved healing efficiency.

Table 4.6: VA.2 welding strength recovery summary

Formulation	Baseline LSS (MPa)	Re-bond LSS (MPa)	Welding LSS (MPa)
VM-AA-CS2	17.81 ($\pm$1.50)	9.33 (53%)	8.17 (47%)

The strength recovery of SW and RB joints highlights the vitrimeric behavior of the VA.2 material. Adhesive (interfacial) failure on both adherends is observed upon re-adhesion and lap shear testing: this failure mode is strong evidence that bond-exchange reactions occur between the adhesive layers during the welding process.

CHAPTER FIVE

CONCLUSIONS

In this work, two epoxy/imine vitrimer formulations originally intended for use as composite matrix – DCN-PEI (VA.1) and a commercial vitrimer formulation (VA.2) – are tested for their performance as reversible vitrimeric adhesives. To characterize the adhesive performance, aluminum (VA.1 and VA.2) and mixed-mixed material AA-CFRP (VA.2 only) SLJs are lap shear tested. Both vitrimer formulations demonstrate good joint strength, ductility, and T_g values when compared to traditional structural epoxy adhesives. Full reversibility performance of the joints is assessed with de-bonding and re-bonding/welding tests. Important results and conclusions for each vitrimer formulation, the author's contribution to the area of research (novel findings), and suggestions for future work, which would complement the findings of this study, are summarized in this chapter.

5.1 DCN-PEI (VA.1)

The VA.1 bulk properties and joint strength are tested for 4 material variations: 2 cure schedules – with (CS1) and without (CS2) a high temperature post-cure – and 2 DCN:PEI monomer ratios - 1:1 and 2:1. The primary conclusions concerning the VA.1 formulation are as follows:

- All tested variations for VA.1 possess good thermomechanical properties, with T_g values ranging from 51 to 83 °C.
- VA.1-2:1-CS2 ratio presents the best bulk characteristics compared to the other VA.1 formulations.
- VA.1-1:1-CS2 shows high moisture uptake and diffusivity D (M_∞ = 48%, D = 9.0E-11 m^2/s). This is accompanied by a loss of mechanical properties that

indicates chemical degradation, as the T_g decreases after hot/wet cycling and desorption (drying).

- High temperature healing of hot/wet cycled vitrimer enables full recovery of the viscoelastic properties, reversing hydrolysis.

- For the VA.1 formulation, the 1:1 monomer ratio and the lower curing temperature (VA.1-1:1-CS2) have the best overall joint performance, yielding a lap shear strength comparable to commercially available structural epoxy adhesives (LSS = 16.5 MPa $\pm$ 5% , d_u = 1.1 mm $\pm$ 46%). The VA.1-2:1-CS2 SLJs have lower LSS, due to high temperature post cure-related adhesive embrittlement.

- VA.1-1:1-CS2 has a fracture toughness (G_{1c}) of 1,819 J/m^2, which is comparable to commercially available toughened epoxy adhesives.

- Creep at 10% of the LSS does not lead to failure. Higher loading ratios cause creep failure within the allotted 20 h, with slightly higher creep rates than commercially available epoxy adhesives.

- VA.1-1:1-CS2 possesses fast relaxation times at elevated temperatures (relaxation time τ = 8 min at 175 °C).

- Heat-driven de-bonding by induction heating is highly repeatable (100% of the tested samples de-bond successfully) and fast (average $t_{de\text{-}bond}$ = 141 s). The top substrate temperature at the time of de-bonding is collected (average $T_{de\text{-}bond}$ = 211 °C).

- Self-welding (SW) upon first adhesion yields a 20% healing efficiency (evidence for the vitrimeric behavior of the adhesive formulation). This strength recovery demonstrates proof-of-concept towards full reversibility for adhesive joints.

Overall, VA.1-1:1-CS2 shows good joint strength; however, the variance in elongation at break is significantly larger than that of structural adhesives. In addition, the high rate of moisture uptake and non-Fickian diffusion observed in VA.1 samples make this formulation less suitable for structural applications. To become viable for reversible structural adhesive applications, further tuning of the adhesive chemistry to improve environmental stability while maintaining joint strength, as well as investigation into the impact that low durability has on reversibility performance, are necessary.

5.2 Commercial Epoxy-Imine Vitrimer (VA.2)

For the commercially available epoxy-imine vitrimer (VA.2), two cure schedules are proposed: CS1 – high temperature (HT) post-cure – and CS2 – no HT post-cure. The key takeaways from the VA.2 experiments are:

- The commercial Epoxy-Imine exhibits exceptional thermomechanical properties and stability for both cure schedules (T_g ~87-101 °C). As for the VA.1 formulation, the T_g and viscoelastic moduli decrease upon the removal of the recommended high temperature post-cure.

- Both SLJ configurations – with fully aluminum (AA) or mixed-material (MM) substrates – have reasonably high strength for structural adhesive applications. MM SLJs have slightly lower strength (16.1-17.0 MPa) than AA joints (17.9-18.0 MPa).

- As with VA.1, the removal of the post-cure causes an increase in SLJ ductility for both joint configurations. However, failure of both cure types is within the same region for aluminum substrates (ductile failure), so the joint strength is governed by the bulk properties (as seen in VA.1-2:1 SLJs).

- Fast de-bonding at low loads is highly repeatable (100% of the tested samples de-bond successfully). De-bonding occurs in less than 3 min (average) for VA.2-AA-CS2 and VA.2-MM-CS2.
- Reversibility is successful for both re-bonded (RB) and self-welded (SW) samples. The average healing efficiency of RB (after de-bonding) specimens is higher than that of SW specimens – 47% and 44%, respectively.

VA.2 is better suited than VA.1 for fully reversible structural adhesive applications: overall, VA.2 joints perform better than VA.1 for both cure schedules and have superior thermomechanical stability. Reversibility tests are also successful, as VA.2 demonstrates fast de-bonding, while obtaining healing efficiency as high as 53% (for RB specimens).

5.3 Novel findings

In this thesis, two existing composite infusion vitrimer resin formulations are adapted for their use as reversible adhesives. In addition, the environmental instability and consequent healing are investigated for the first time for the VA.1 formulation. A detailed summary of the novel contributions is included below:

- Cure schedule modification: removal of high temperature post-cure phase leads to higher elongation at break, which in turn promotes ductile failure and higher LSS.
- De-bonding tests: fast, heat-driven de-bonding, as well as precise de-bonding time and substrate temperature collection are made possible by induction heating. This is the first reported attempt to collect this data during heat-driven de-bonding of vitrimeric adhesive joints.
- Moisture uptake: the high moisture uptake of DCN-PEI is not reported in the literature. Hydrolysis of the DCN-PEI vitrimer (and its effects on the viscoelastic properties) is found to be reversible through low RH, heat-induced self-healing.

5.4 Future work

Research on vitrimeric adhesives is still in its infancy, so there are many questions that remain unanswered. Further investigation is recommended to expand upon the results of this study. Bulk and joint characterization of the tensile properties, stress-relaxation, SLJ creep, thermal expansion (dilatometry), and Mode I fracture toughness can be expanded to encompass more combinations of mix ratio and cure schedule for both vitrimer formulations. In addition, Mode II fracture toughness – using end-notch flexure (ENF) specimens – as well as creep performance – for both bulk (tension film) specimens and within a thick adherend shear test (TAST) joint – should be investigated.

Deeper investigation of the mechanism driving the relationship between moisture uptake and joint performance for VA.1 samples is needed, with greater focus on measuring and controlling the environmental conditions during synthesis, cure, storage, and testing. For this purpose, temperature and humidity conditions should be tracked during the entire samples life cycle, joints should be cured in an environmental chamber at 0% RH, additional controlled environmental aging of SLJs and spectroscopy of the aged samples should be performed. Studying the reversibility performance of aged bulk VA.1 samples would also be of interest, to quantify the effect of moisture uptake on de-bonding and re-bonding. Submersion tests of VA.2 would also help to confirm its environmental stability and to compare it to VA.1.

More investigation into the reversibility of SLJs is worthwhile; priority should be given to increasing the sample size, optimizing the weld parameters, and studying the effect of the adhesive surface topography on the welding efficiency. Sequential reversibility (i.e. after multiple cycles of de-bonding and re-bonding) should also be studied to determine the effect of repeated heat-exposure on the healing efficiency. Finally, the temperature of the adhesive layer during de-bonding tests is not measured in this thesis: thermocouples could be embedded in the bondline, but would be subjected to

direct induction heating, rendering their output unreliable. Therefore, the development of a novel methodology to measure the temperature of the adhesive during induction-driven de-bonding tests – either via direct measurement or via inference from substrate data – would significantly advance the understanding of the de-bonding mechanism, and would serve as an important tool to optimize reversibility parameters.

REFERENCES

[1] P. Mallick, *Materials, design and manufacturing for lightweight vehicles*. Mar. 2010.

[2] T. Go, D. Wahab, M. Rahman, R. Ramli, and C. Azhari, "Disassemblability of end-of-life vehicle: a critical review of evaluation methods," *Journal of Cleaner Production*, vol. 19, no. 13, pp. 1536–1546, 2011.

[3] European Parliament and Council, "Directive 2000/53/EC of 18 September 2000 on end-of life vehicles," *Official Journal of the European Communities*, pp. 34–42, 2000. OJ L 269, 18 September 2000, p. 34-42.

[4] European Parliament and of the Council, "Regulation (eu) 2023/851 of the european parliament and of the council of 19 april 2023 amending regulation (eu) 2019/631 as regards strengthening the co2 emission performance standards for new passenger cars and new light commercial vehicles in line with the union's increased climate ambition," *Official Journal of the European Union*, vol. L 110, p. 5–20.

[5] T. Domenech and B. Bahn-Walkowiak, "Transition towards a resource efficient circular economy in europe: Policy lessons from the eu and the member states," *Ecological Economics*, vol. 155, pp. 7–19, Mar. 2019.

[6] A. Candela, G. Sandrini, M. Gadola, D. Chindamo, and P. Magri, "Lightweighting in the automotive industry as a measure for energy efficiency: Review of the main materials and methods," *Heliyon*, vol. 10, no. 8, p. e29728, 2024.

[7] A. L. Robinson, A. I. Taub, and G. A. Keoleian, "Fuel efficiency drives the auto industry to reduce vehicle weight," *Energy Quarterly*, vol. 44, no. 12, pp. 920–923, 2019.

[8] L. F. M. da Silva, A. Öchsner, and R. D. Adams, "Introduction to adhesive bonding technology," in *Handbook of Adhesion Technology* (L. F. M. da Silva, A. Öchsner, and R. D. Adams, eds.), pp. 1–7, Cham: Springer International Publishing, 2018.

[9] S. Omairey, N. Amirth Jayasree, and M. Kazilas, "Defects and uncertainties of adhesively bonded composite joints," *SN Applied Sciences*, vol. 3, Sept. 2021.

[10] F. Bellucci, L. Nicodemo, A. Bongiovanni, A. Martino, and G. Capobianco, "Galvanic corrosion at composite-metallic materials interface," *Key Engineering Materials*, vol. 20-28, pp. 633–641, Jan. 1988.

[11] C. Zhang, D. Zheng, G.-L. Song, Y. Guo, M. Liu, and H. Kia, "Corrosion behavior of the joints of carbon fiber reinforced polymers with dp590 steel and al6022 alloy," *Anti-Corrosion Methods and Materials*, vol. ahead-of-print, Jul. 2019.

[12] M. Banea and L. da Silva, "Adhesively bonded joints in composite materials: An overview," *Proceedings of The Institution of Mechanical Engineers Part L-journal of Materials-design and Applications - PROC INST MECH ENG L-J MATER*, vol. 223, pp. 1–18, Jan. 2009.

[13] C. Sato, "Recycling and environmental aspects," in *Handbook of Adhesion Technology* (L. F. M. da Silva, A. Öchsner, and R. D. Adams, eds.), pp. 1751–1774, Cham: Springer International Publishing, 2018.

[14] D. E. Packham, "Theories of fundamental adhesion," in *Handbook of Adhesion Technology* (L. F. M. da Silva, A. Öchsner, and R. D. Adams, eds.), pp. 11–41, Cham: Springer International Publishing, 2018.

[15] "Benchmarking of potential rapid inspection methods for quantitative tracking of ambient ageing in aerospace prepregs," *Composites Part B: Engineering*, vol. 254, p. 110579, 2023.

[16] G. Critchlow, "General introduction to surface treatments," in *Handbook of Adhesion Technology* (L. F. M. da Silva, A. Öchsner, and R. D. Adams, eds.), pp. 131–161, Cham: Springer International Publishing, 2018.

[17] "Standard test method for apparent shear strength of single-lap-joint adhesively bonded metal specimens by tension loading (metal-to-metal)," Tech. Rep. D1002, 2019. <organization>ASTM International</organization>, <location>West Conshohocken, PA>.

[18] R. Adams, J. Comyn, and W. Wake, *Structural adhesive joints in engineering*. United Kingdom: Chapman and Hall, 1997. Other: 2nd Edition.

[19] E. Sancaktar, "Classification of adhesive and sealant materials," in *Handbook of Adhesion Technology* (L. F. M. da Silva, A. Öchsner, and R. D. Adams, eds.), pp. 283–317, Cham: Springer International Publishing, 2018.

[20] M. Banea, "Debonding on demand of adhesively bonded joints: A critical review," *Reviews of Adhesion and Adhesives*, vol. 7, pp. 33–50, Mar. 2019.

[21] J. Goodenough, A. Fitzgerald, K. Bean, J. Hatcliffe, A. Slark, I. Hamerton, and I. Bond, "Reversible adhesives and debondable joints for fibre-reinforced plastics: Characteristics, capabilities, and opportunities," *Materials Chemistry and Physics*, vol. 299, p. 127464, 2023.

[22] M. Banea, L. da Silva, R. Carbas, and R. Campilho, "Mechanical and thermal characterization of a structural polyurethane adhesive modified with thermally expandable particles," *International Journal of Adhesion and Adhesives*, vol. 54, pp. 191–199, 2014.

[23] M. D. Banea, L. F. M. da Silva, R. J. C. Carbas, and R. D. Campilho, "Structural adhesives modified with thermally expandable particles," *The Journal of Adhesion*, vol. 91, no. 10-11, pp. 823–840, 2015.

[24] M. Banea, L. da Silva, and R. Carbas, "Debonding on command of adhesive joints for the automotive industry," *International Journal of Adhesion and Adhesives*, vol. 59, pp. 14–20, 2015.

[25] M. Banea, L. Silva, R. Carbas, and S. de Barros, "Debonding on command of multi-material adhesive joints," *The Journal of Adhesion*, vol. 93, Jun. 2016.

[26] M. Banea, L. da Silva, R. Carbas, A. Barbosa, S. de Barros, and G. Viana, "Effect of water on the behaviour of adhesives modified with thermally expandable particles," *International Journal of Adhesion and Adhesives*, vol. 84, pp. 250–256, 2018.

[27] G. Piazza, M. Burczyk, M. Gerini-Romagnoli, G. Belingardi, and S. A. Nassar, "Effect of thermally expandable particle additives on the mechanical and reversibility performance of adhesive joints," *Journal of Advanced Joining Processes*, vol. 5, p. 100088, 2022.

[28] K. Tedlapu and M. Gerini-Romagnoli, "Improved de-bonding of composite adhesive joints with bondline inserts," Jan. 2025.

[29] 3M Industrial Adhesives and Tapes Division, "Choosing and using a structural adhesive," white paper, 3M Company, 2012.

[30] P. Kraisornkachit, M. Mano, K. Hitomi, S. Horiuchi, and M. Naito, "Biomimetic hot-melt adhesive using galloyl-grafted polypropylene for multisubstrates," *ACS Applied Polymer Materials*, vol. 8, no. 13, pp. 10668–10679, 2026.

[31] J. Zheng, N. J. Galan, M. Boucher, O. Jupp, M. S. Karunarathna, J. Choi, C. C. Kehelkadu Withanage, T. L. Nelson, J. C. Foster, and T. Saito, "Tailored glycolysis of nylon 6 to enable upcycling into high-strength adhesives," *Cell Reports Physical Science*, vol. 6, no. 11, p. 102908, 2025.

[32] G.-L. Davies, J. Govan, R. Tekoriute, R. Serrano-García, H. Nolan, D. Farrell, O. Hajatpour, and Y. K. Gun'ko, "Magnetically activated adhesives: towards on-demand magnetic triggering of selected polymerisation reactions," *Chem. Sci.*, vol. 8, pp. 7758–7764, 2017.

[33] X. Cheng, Y. Zhou, A. D. Charles, Y. Yu, M. S. Islam, S. Peng, J. Wang, A. N. Rider, M. Lim, V. Timchenko, and C.-H. Wang, "Enabling contactless rapid on-demand debonding and rebonding using hysteresis heating of ferrimagnetic nanoparticles," *Materials & Design*, vol. 210, p. 110076, 2021.

[34] Y. Sun, M. Wang, Q. Zheng, Z. Zhang, Y. Li, Z. Cheng, W. Jiang, and C. Zhang, "Nanoparticles: Excellent materials yet dangerous when they become airborne," *Toxics*, vol. 10, no. 2, p. 50, 2022.

[35] D. S. Allan, J. P. Bell, M. Cooney, M. McBrearty, and H. P. Silverman, "Electrelease–electrically disbonding epoxy adhesive," *Assembly Automation*, vol. 22, no. 4, pp. 326–331, 2002.

[36] W. Alabiso and S. Schlögl, "The impact of vitrimers on the industry of the future: Chemistry, properties and sustainable forward-looking applications," *Polymers*, vol. 12, no. 8, 2020.

[37] X. Cui, N. Jiang, J. Shao, H. Zhang, Y. Yang, and P. Tang, "Linear and nonlinear viscoelasticities of dissociative and associative covalent adaptable networks: Discrepancies and limits," *Macromolecules*, vol. 56, no. 3, pp. 772–784, 2023.

[38] C. Bowman, F. Du Prez, and J. Kalow, "Introduction to chemistry for covalent adaptable networks," *Polymer Chemistry*, vol. 11, Jul. 2020.

[39] D. Montarnal, M. Capelot, F. Tournilhac, and L. Leibler, "Silica-like malleable materials from permanent organic networks," *Science*, vol. 334, no. 6058, pp. 965–968, 2011.

[40] M. Capelot, M. M. Unterlass, F. Tournilhac, and L. Leibler, "Catalytic control of the vitrimer glass transition," *ACS Macro Letters*, vol. 1, no. 7, pp. 789–792, 2012. PMID: 35607118.

[41] F. Meng, M. O. Saed, and E. M. Terentjev, "Rheology of vitrimers," *Nature Communications*, vol. 13, no. 1, p. 5753, 2022.

[42] R. Young and P. Lovell, *Introduction to Polymers: Third Edition*. United States: CRC Press, 3 ed., Jun. 2011.

[43] Pekaje, "Maxwell model for viscoelastic materials.." [Online], Apr. 2007. Public Domain. Accessed via Wikipedia.

[44] L. Zhang, X. Tian, M. H. Malakooti, and H. A. Sodano, "Novel self-healing cfrp composites with high glass transition temperatures," *Composites Science and Technology*, vol. 168, pp. 96–103, 2018.

[45] Y. Yang, Y. Xu, Y. Ji, and Y. Wei, "Functional epoxy vitrimers and composites," *Progress in Materials Science*, vol. 120, p. 100710, 2021.

[46] X. Feng and G. Li, "Room-temperature self-healable and mechanically robust thermoset polymers for healing delamination and recycling carbon fibers," *ACS Applied Materials & Interfaces*, vol. 13, no. 44, pp. 53099–53110, 2021. PMID: 34705416.

[47] H. Sharma, M. Bender, G. Kim, D. Lee, C. Caglayan, S. Schlögl, G. J. Yun, A. Kumar, and S. Rana, "Reprocessable carbon fiber vitrimer composites: Reclamation and reformatting of carbon fibers for second generation composite materials," *Journal of Applied Polymer Science*, vol. 141, no. 41, p. e56074, 2024.

[48] V. Schenk, K. Labastie, M. Destarac, P. Olivier, and M. Guerre, "Vitrimer composites: current status and future challenges," *Materials Advances*, vol. 3, no. 22, pp. 8012–8029, 2022.

[49] Y. Sun, M. Wang, Z. Wang, Y. Mao, L. Jin, K. Zhang, Y. Xia, and H. Gao, "Amine-cured glycidyl esters as dual dynamic epoxy vitrimers," *Macromolecules*, vol. 55, no. 2, pp. 523–534, 2022. LSS up to 4 MPa for bonding Aluminum Sheets.

[50] A. Trejo-Machin, L. Puchot, and P. Verge, "A cardanol-based polybenzoxazine vitrimer: recycling, reshaping and reversible adhesion," *Polym. Chem.*, vol. 11, pp. 7026–7034, 2020.

[51] Z. Zhou, X. Su, J. Liu, and R. Liu, "Synthesis of vanillin-based polyimine vitrimers with excellent reprocessability, fast chemical degradability, and adhesion," *ACS Applied Polymer Materials*, vol. 2, no. 12, pp. 5716–5725, 2020. LSS up to 6.4 MPa for bonding iron.

[52] J. Tang, L. Wan, Y. Zhou, H. Pan, and F. Huang, "Strong and efficient self-healing adhesives based on dynamic quaternization cross-links," *J. Mater. Chem. A*, vol. 5, pp. 21169–21177, 2017.

[53] X. Zhang, S. Wang, Z. Jiang, Y. Li, and X. Jing, "Boronic ester based vitrimers with enhanced stability via internal boron–nitrogen coordination," *Journal of the American Chemical Society*, vol. 142, no. 52, pp. 21852–21860, 2020. PMID: 33332118.

[54] D. Santiago, D. Guzman, J. Padilla, P. Verdugo, S. De la Flor, and À. Serra, "Recyclable and reprocessable epoxy vitrimer adhesives," *ACS Applied Polymer Materials*, vol. 5, no. 3, pp. 2006–2015, 2023.

[55] M. Surós, D. Santiago, P. Verdugo, M. Pedrola, and S. D. la Flor, "Reversible adhesives from epoxy-based transesterification-induced vitrimers," *Polymer*, vol. 299, p. 126939, 2024.

[56] A. Roig, L. Molina, A. Serra, D. Santiago, and S. De la Flor, "Structural reversible adhesives based on thiol-epoxy vitrimers," *Polymer Testing*, vol. 128, p. 108205, 2023.

[57] P. Verdugo, D. Santiago, S. De la Flor, and A. Serra, "A biobased epoxy vitrimer with dual relaxation mechanism: A promising material for renewable, reusable, and

recyclable adhesives and composites," *ACS Sustainable Chemistry & Engineering*, vol. 12, no. 15, pp. 5965–5978, 2024.

[58] A. Dong, Q. Liu, H. Yao, J. Ma, J. Cheng, and J. Zhang, "Epoxy vitrimer with excellent mechanical properties and high t g for detachable structural adhesives," *ACS Applied Materials & Interfaces*, vol. 17, no. 9, pp. 14578–14590, 2025.

[59] A. Vilanova-Perez, M. Suros, A. Serra, S. De la Flor, and A. Roig, "Custom-shaped malleable, recyclable and reversible structural adhesives based on vanillin polyimine vitrimers," *Reactive and Functional Polymers*, vol. 206, p. 106109, 2025.

[60] S. Nartam, S. Budhe, J. Paul, and S. de Barros, "Strength, repairability, and debonding of vitrimer structural adhesive joints," *Academia Materials Science*, vol. 3, no. 2, 2026.

[61] D. Lee, J.-H. Kim, S. B. Yang, and D.-J. Kwon, "Development of reprocessable structural adhesives based on covalent adaptable networks for wind turbine blade," *Composites Part B: Engineering*, vol. 301, p. 112519, 2025.

[62] O. Tetteh, P. Mensah, and G. Li, "Repeated healing of low velocity impact induced damage in orthogrid-stiffened sandwich panel," *Journal of Composite Materials*, vol. 57, pp. 3619–3632, Sept. 2023.

[63] B. Mahoney, O. Tetteh, K. Y. Gyabaah, P. Mensah, J. W. Gillespie Jr, and G. Li, "Effect of healing parameters on the healing efficiency of a vitrimer," *Journal of Applied Polymer Science*, vol. 142, no. 46, p. e57810, 2025. e57810 app.20251774.

[64] ASTM International, "Standard Test Method for Tensile Properties of Plastics," Standard ASTM D638, ASTM International, West Conshohocken, PA, 2014.

[65] L. F. M. da Silva, E. A. S. Marques, and R. D. S. G. Campilho, "Design rules and methods to improve joint strength," in *Handbook of Adhesion Technology* (L. F. M. da Silva, A. Öchsner, and R. D. Adams, eds.), pp. 773–810, Cham: Springer International Publishing, 2018.

[66] L. Silva, T. Rodrigues, M. de Figueiredo, M. De Moura, and J. Chousal, "Effect of adhesive type and thickness on the lap shear strength," *The Journal of Adhesion*, vol. 82, pp. 1091–1115, Oct. 2006.

[67] ASTM International, "Standard test method for fracture strength in cleavage of adhesives in bonded metal joints," standard, West Conshohocken, PA, 2020.

[68] Strafpeloton2, "Strain as a function of time due to constant stress over an extended period for a viscoelastic material. the three stages of material creep behavior - primary, secondary, tertiary.." Online Image, Oct. 2009. Public Domain. Accessed via Wikipedia.

[69] F. Ceroni, M. Pecce, C. Carloni, T. Leusmann, H. Budelmann, E. Nigro, A. Bilotta, J. Barros, I. Costa, G. P. Lignola, A. Napoli, and R. Realfonzo, "Special problems," pp. 195–262, 08 2015.

[70] B. C. Duncan, J. M. Urquhart, and S. Roberts, "Review of measurement and modelling of permeation and diffusion in polymers," Tech. Rep. DEPC-MPR 012, National Physical Laboratory (NPL), Jan. 2005.

[71] K. Whitcomb, "Frequency dependence of glass transition temperatures," tech. rep., TA Instruments, New Castle, DE, USA, 2026.

[72] A. F. Abdelkader and J. R. White, "Water absorption in epoxy resins: The effects of the crosslinking agent and curing temperature," *Journal of Applied Polymer Science*, vol. 98, no. 6, pp. 2544–2549, 2005.

[73] P. Taynton, K. Yu, R. K. Shoemaker, Y. Jin, H. J. Qi, and W. Zhang, "Heat- or water-driven malleability in a highly recyclable covalent network polymer," *Advanced Materials*, vol. 26, no. 23, pp. 3938–3942, 2014.

[74] I. A. Ashcroft, J. Comyn, and A. Mubashar, "Effect of water and mechanical stress on durability," in *Handbook of Adhesion Technology* (L. F. M. da Silva, A. Öchsner, and R. D. Adams, eds.), pp. 879–914, Cham: Springer International Publishing, 2018.

[75] A. F. Abdelkader and J. R. White, "Water absorption in epoxy resins: The effects of the crosslinking agent and curing temperature," *Journal of Applied Polymer Science*, vol. 98, no. 6, pp. 2544–2549, 2005.

[76] M. Waqas, C. Robert, U. Arif, N. Radacsi, D. Ray, and V. Koutsos, "Improving the through-thickness electrical conductivity of carbon fiber reinforced polymer composites using interleaving conducting veils," *Journal of Applied Polymer Science*, vol. 139, no. 43, p. e53060, 2022.